Article

Cell Chemical Biology

Selective killing of the human gastric pathogen *Helicobacter pylori* by mitochondrial respiratory complex I inhibitors

Graphical abstract

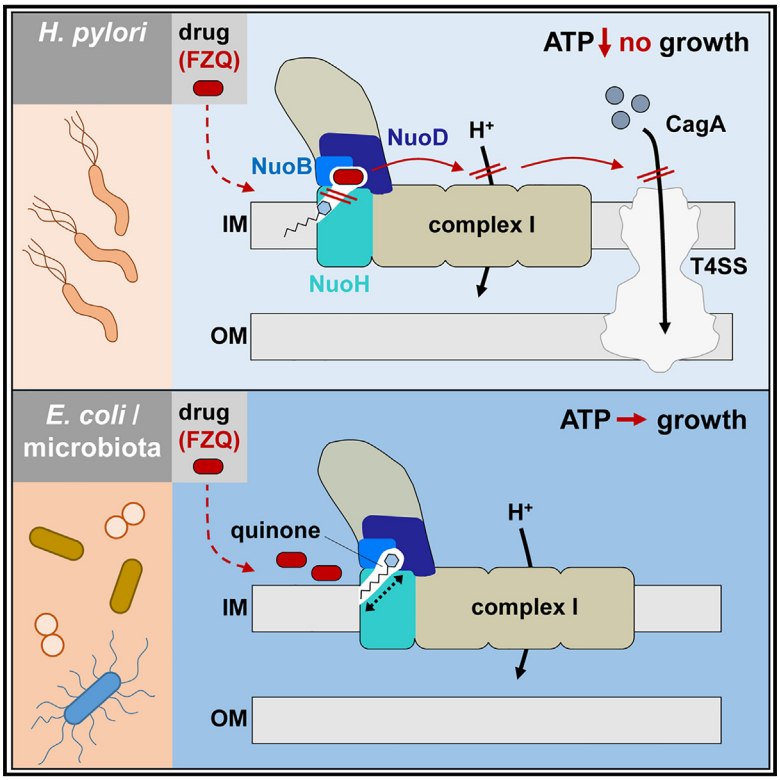

Highlights

- T4SS reporter screening identifies species-specific *H. pylori* growth inhibitors
- Inhibitors specifically target NuoB and NuoD of *H. pylori*'s respiratory complex I
- A unique quinone-binding pocket explains *H. pylori*'s extreme inhibitor sensitivity
- Molecular modeling of the quinone-binding site enables rational inhibitor design

Authors

Clara Lettl, Franziska Schindele, Ahmad Reza Mehdipour, ..., Matthias Witschel, Wolfgang Fischer, Rainer Haas

Correspondence

fischer@mvp.lmu.de (W.F.), haas@mvp.lmu.de (R.H.)

In brief

Lettl et al. report that the unique composition of respiratory complex I in *H. pylori* makes these bacteria extremely susceptible to small-molecule inhibitors targeting the complex I quinone-binding pocket, while intestinal bacteria remain unaffected, providing an opportunity to develop selective antibacterial drugs.

Lettl et al., 2023, Cell Chemical Biology *30*, 499–512
May 18, 2023
https://doi.org/10.1016/j.chembiol.2023.04.003

CellPress

Cell Chemical Biology

CellPress

Article

Selective killing of the human gastric pathogen *Helicobacter pylori* by mitochondrial respiratory complex I inhibitors

Clara Lettl,[1,2] Franziska Schindele,[1,2] Ahmad Reza Mehdipour,[3,4] Thomas Steiner,[5] Diana Ring,[1] Ruth Brack-Werner,[2,6] Bärbel Stecher,[1,2] Wolfgang Eisenreich,[5] Ursula Bilitewski,[7,8] Gerhard Hummer,[4,9] Matthias Witschel,[10] Wolfgang Fischer,[1,2,11,12,*] and Rainer Haas[1,2,11,*]

[1]Max von Pettenkofer Institute of Hygiene and Medical Microbiology, Faculty of Medicine, LMU Munich, Pettenkoferstrasse 9a, 80336 Munich, Germany
[2]German Center for Infection Research (DZIF), Partner Site Munich, Munich, Germany
[3]Center for Molecular Modeling, Ghent University, 9052 Zwijnaarde, Belgium
[4]Department of Theoretical Biophysics, Max Planck Institute of Biophysics, 60438 Frankfurt am Main, Germany
[5]Bavarian NMR Center-Structural Membrane Biochemistry, Department of Chemistry, Technical University Munich, 85748 Garching, Germany
[6]German Research Center for Environmental Health, Institute of Virology, Helmholtz Center Munich, 85764 Neuherberg, Germany
[7]Helmholtz Center for Infection Research, 38124 Braunschweig, Germany
[8]German Center for Infection Research (DZIF), Partner Site Hannover/Braunschweig, Braunschweig, Germany
[9]Institute for Biophysics, Goethe University Frankfurt, 60438 Frankfurt am Main, Germany
[10]BASF SE, 67056 Ludwigshafen, Germany
[11]Senior author
[12]Lead contact
*Correspondence: fischer@mvp.lmu.de (W.F.), haas@mvp.lmu.de (R.H.)
https://doi.org/10.1016/j.chembiol.2023.04.003

SUMMARY

Respiratory complex I is a multicomponent enzyme conserved between eukaryotic cells and many bacteria, which couples oxidation of electron donors and quinone reduction with proton pumping. Here, we report that protein transport via the Cag type IV secretion system, a major virulence factor of the Gram-negative bacterial pathogen *Helicobacter pylori*, is efficiently impeded by respiratory inhibition. Mitochondrial complex I inhibitors, including well-established insecticidal compounds, selectively kill *H. pylori*, while other Gram-negative or Gram-positive bacteria, such as the close relative *Campylobacter jejuni* or representative gut microbiota species, are not affected. Using a combination of different phenotypic assays, selection of resistance-inducing mutations, and molecular modeling approaches, we demonstrate that the unique composition of the *H. pylori* complex I quinone-binding pocket is the basis for this hypersensitivity. Comprehensive targeted mutagenesis and compound optimization studies highlight the potential to develop complex I inhibitors as narrow-spectrum antimicrobial agents against this pathogen.

INTRODUCTION

Infection with the human gastric pathogen *Helicobacter pylori* is arguably the most common chronic bacterial infection in humans, with an overall number of infected individuals probably exceeding 4 billion people.[1] Through its association with diseases such as atrophic gastritis, peptic ulcer disease, and gastric cancer, colonization with *H. pylori* represents one of the leading causes of infection-associated morbidity and mortality worldwide. Thus, it has been estimated that over 800,000 new cases of gastric cancer per year are attributable to *H. pylori* infection.[2] Due to its causative relationship with cancer development, *H. pylori* has been classified by the WHO as a definitive (class I) carcinogen.[3] The immune system is not able to clear the infection, resulting in the characteristic gastric inflammation that persists for decades if untreated.[4] Commonly used triple or quadruple therapies to eradicate *H. pylori* face the challenge of increasing resistance rates,[5–7] so that *H. pylori*, particularly with clarithromycin resistance, has been listed by the WHO as a high-priority pathogen for research and development of new antibiotics.[8] Thus, novel concepts and novel therapeutics are required to either replace or complement the established treatment schemes. Such novel treatment concepts may include the use of dual-target antibiotics composed of existing structures[9] or the identification of narrow-spectrum or species-specific antimicrobial agents with novel targets,[10,11] but also non-classical approaches such as antivirulence compounds designed to inhibit pathogenicity factors without affecting bacterial viability.[12–15]

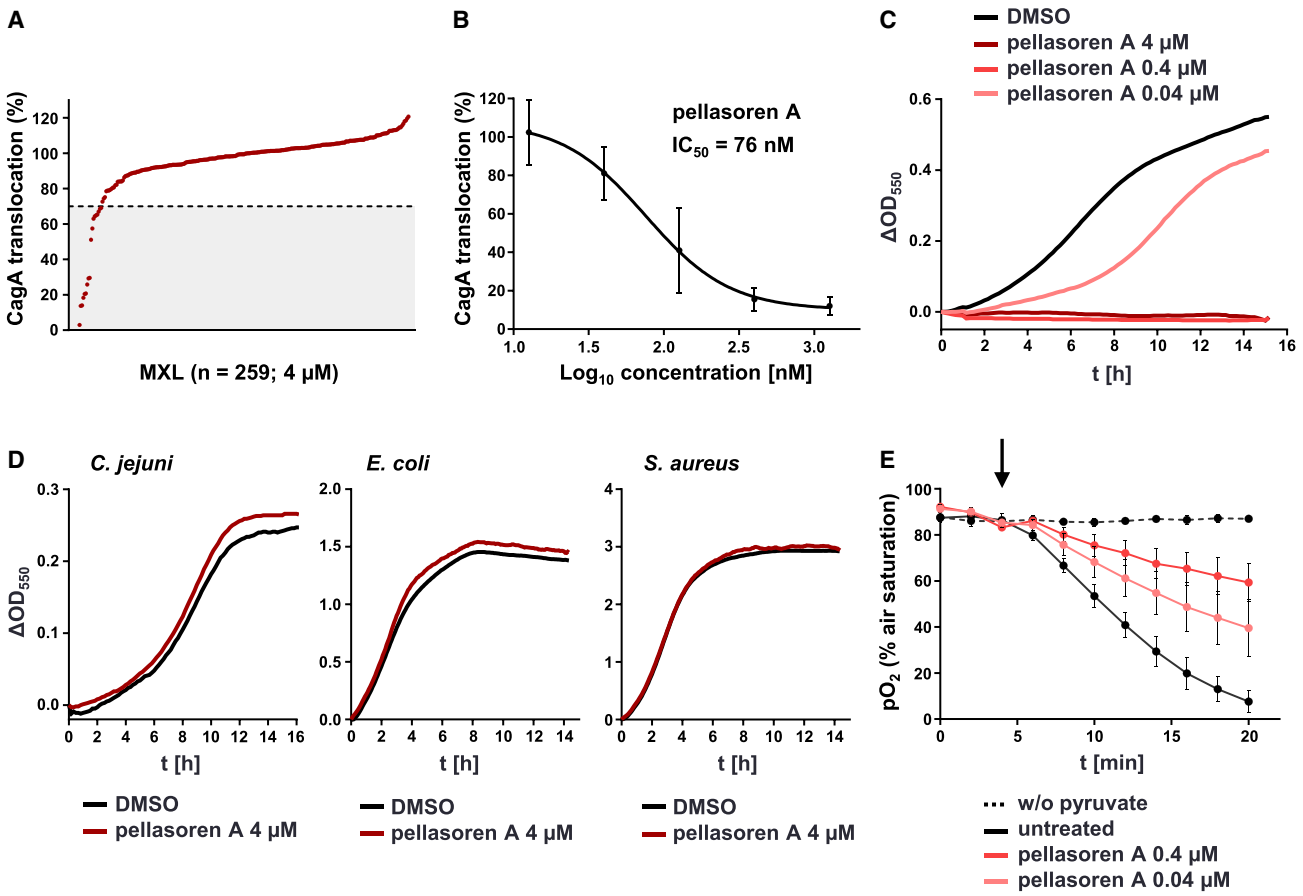

Figure 1. Identification of myxobacterial secondary metabolites with selective growth-inhibitory properties against *H. pylori*

(A) Results of screening the MXL library with the TEM-1-CagA translocation reporter assay. Individual compounds are shown as dots in ascending order with respect to the resulting CagA translocation rates (indicated as percentage of untreated control).

(B) Dose-response curve of pellasoren A obtained with the TEM-1-CagA translocation reporter assay (using the BAC approach; compare Figure S1). Data represent mean values and standard deviations of four independent measurements.

(C) Growth of *H. pylori* P12 was monitored as optical density at 550 nm (OD_{550}) in the absence or presence of the indicated concentrations of pellasoren A.

(D) Growth of *C. jejuni* C31, *E. coli* Top10, and *S. aureus* ATCC29213 in the presence or absence of pellasoren A.

(E) Strain P12 was treated with the indicated inhibitor concentrations for 10 min in OxoPlates or left untreated. Subsequently, partial oxygen pressures (pO_2) were recorded over 20 min, and pyruvate was injected after 4 min (arrow) to a final concentration of 7 mM. Data represent mean values and standard errors of the mean (SEM) obtained from four independent experiments. See also Figures S1 and S2 and Tables S1 and S2.

In the case of *H. pylori*, a promising target for the development of antivirulence compounds (pathoblockers) is the type IV secretion system (T4SS) encoded on the cytotoxin-associated gene (*cag*) pathogenicity island.[16] This secretion system stimulates NF-κB-dependent proinflammatory responses in target cells[16] and injects the bacterial protein CagA into the host cell cytoplasm, which is considered a key event in the induction of *H. pylori*-associated disease, particularly gastric cancer.[17] Generally, bacterial T4SSs are widespread machineries for macromolecule (DNA and/or protein) transport, but their compositions and structures are highly diverse.[18] Nevertheless, previous attempts have focused on the development of small-molecule inhibitors targeting conjugative or protein-translocating T4SSs (reviewed in Boudaher and Shaffer[19]), and several compounds inhibiting either Cag T4SS-associated phenotypes or the activity of its VirB11-like ATPase Cagα have been identified.[20–24]

Type IV secretion activity of the Cag system is commonly monitored by measuring tyrosine phosphorylation of its effector protein CagA, which is not suitable for screening compound libraries. To overcome this limitation, we have recently developed reporter assays based on β-lactamase or split-luciferase (HiBiT) fusions to CagA to quantify effector protein translocation in endpoint or real-time settings.[24–26] Here, using the TEM-1-CagA β-lactamase reporter assay, we have identified several compounds from a myxobacterial secondary metabolite library with extremely high potency to inhibit the Cag T4SS, and we show that they act indirectly by targeting the bacterial respiratory chain. Furthermore, we show a generally high sensitivity of *H. pylori*, and the Cag T4SS, to inhibition of respiratory complex I, which is based on the distinct composition of its quinone-binding pocket. Our results demonstrate the potential of targeting *H. pylori* complex I for the development of selective, or narrow-spectrum, inhibitors (pathogen blockers) against this infectious agent.

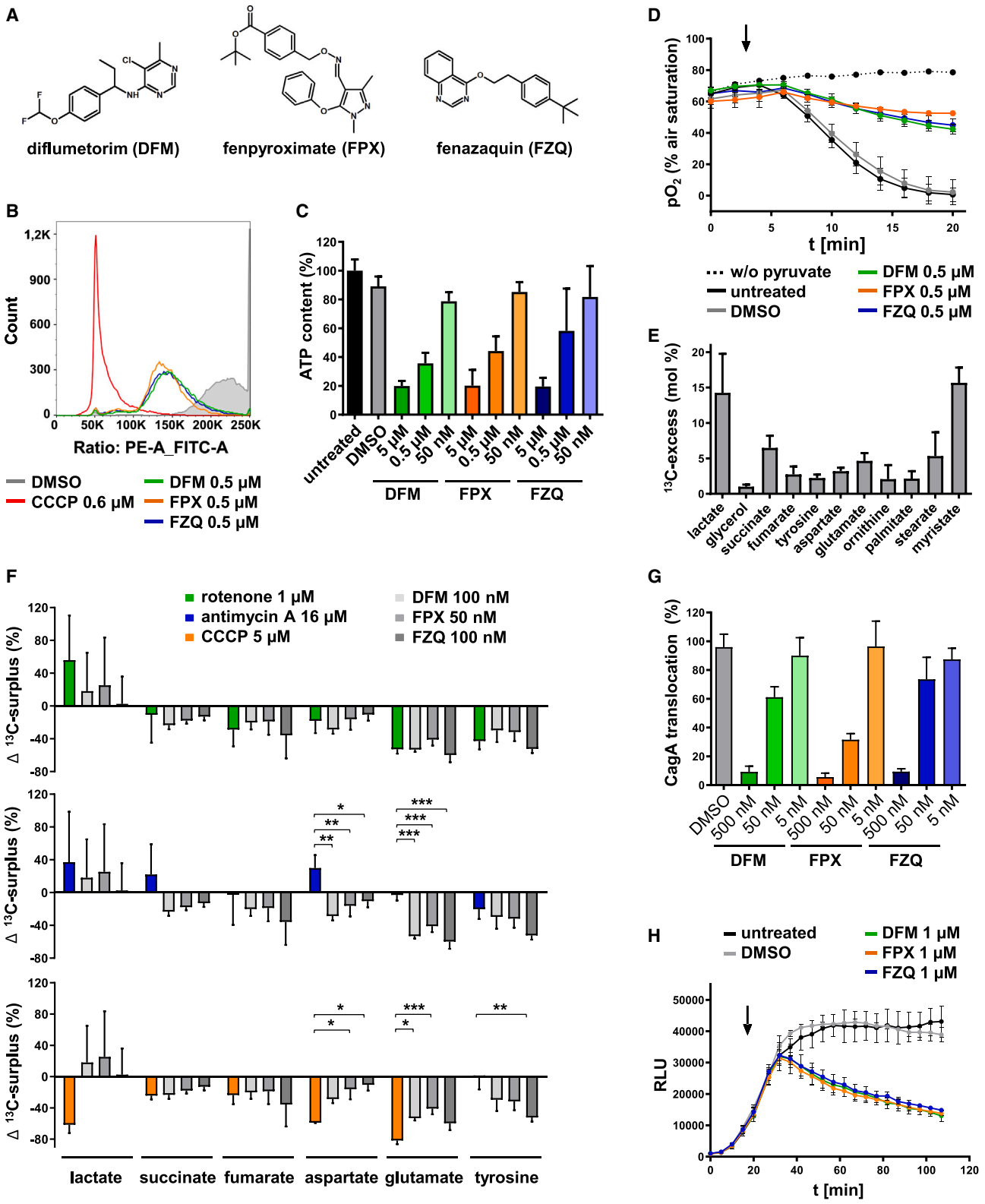

(legend on next page)

RESULTS

Screening of a natural compound library with a type IV secretion reporter identifies substances with species-specific growth-inhibitory characteristics

We have recently developed a β-lactamase-based type IV secretion reporter assay for efficient quantification of CagA translocation into gastric epithelial cells[25] and adapted it to 96-well or 384-well formats to screen small-molecule libraries for potential inhibitors of this process[24] (Figure S1A). We used this downscaled protocol here to screen a myxobacterial secondary metabolite library (MXL library), which is highly enriched in compounds with potent bioactivities.[27] This procedure resulted in the identification of 18 substances inhibiting CagA translocation by at least 30% (Figure 1A and Table S1). All identified compounds were retested at varying concentrations with the β-lactamase reporter assay, using different pre-incubation and washing protocols to distinguish between bacterial and eukaryotic cell targets (Figure S1A) and to eliminate compounds with eukaryotic cell (Figure S1B) or low-potency bacterial targets (Figure S1C). Remarkably, all remaining compounds showed a very high activity in dose-response curves for type IV secretion inhibition, typically in the nanomolar range (Figures 1B and S1D). Counter-screening to determine the impact on *H. pylori* growth demonstrated that all compounds act as growth inhibitors as well, with similar high potencies (Figures 1C and S2 and Table S2). To examine whether they interfere more generally with bacterial viability or fitness, we recorded growth curves of representative Gram-negative and Gram-positive bacteria (*Campylobacter jejuni*, *Escherichia coli*, and *Staphylococcus aureus*) in the absence or presence of these compounds. Surprisingly, most compounds had no inhibitory effects, or only at micromolar concentrations, on the growth of these bacteria, despite their very low IC_{50} values against *H. pylori* (Figures 1D and S2 and Table S2), indicating that *H. pylori* and its Cag T4SS are specifically sensitive to this group of compounds.

Potent type IV secretion inhibition is caused by interference with *H. pylori* respiratory complex I

Most of the active myxobacterial compounds identified above have been described as mitochondrial respiratory chain inhibitors (Table S1). Since *H. pylori* operates a respiratory chain, while containing a reduced set of corresponding enzymes and an atypical complex I assembly,[28,29] we asked whether mitochondrial respiratory inhibitors may generally have a potent and selective activity against *H. pylori.* First, we confirmed that the myxobacterial compounds, including pellasoren A, which has not been described as a respiration inhibitor so far, interfere with respiratory activity in *H. pylori*. Since *H. pylori* is able to run an oxidative tricarboxylic acid (TCA) cycle,[30] and reportedly utilizes substrates such as pyruvate or lactate by respiratory activity,[31] we incubated *H. pylori* cultures in the presence or absence of myxobacterial compounds, then added pyruvate, and monitored oxygen levels using microtiter plates with oxygen sensors (OxoPlates). Indeed, injection of pyruvate resulted in rapidly declining oxygen pressures over a time course of 10–15 min, indicating effective metabolism of this substrate by respiration (Figure 1E). In the presence of pellasoren A, or other myxobacterial respiratory chain inhibitors (data not shown), oxygen consumption was abolished, consistent with aerobic respiration as a target of these compounds.

Next, we determined the sensitivity of *H. pylori* to standard respiratory chain inhibitors (rotenone, antimycin A), the protonophore carbonyl cyanide *m*-chlorophenylhydrazone (CCCP), or other mitochondrial complex I or III inhibitors. Consistent with the observations described above, rotenone and other complex I inhibitors resulted in growth inhibition of *H. pylori* (Table S3), often in the nanomolar range and thus at a potency comparable to that of the myxobacterial compounds, whereas the growth of *C. jejuni*, *E. coli*, or *S. aureus* was not influenced at the same concentrations. This suggested that respiratory chain inhibitors from different compound classes, and complex I inhibitors in particular, are generally active in a species-selective manner against *H. pylori*. Since the myxobacterial compounds are less amenable to chemical modification, we focused our further analysis on the high-potency compounds diflumetorim (DFM), fenpyroximate (FPX), and fenazaquin (FZQ) (Figure 2A), three complex I inhibitors with a fungicidal or acaricidal activity spectrum (Table S3), for which a large number of compound analogs are available. To characterize the impact of these substances on bacterial physiology, we determined the membrane potential and quantified the bacterial ATP content. Administration of any of these compounds resulted in membrane potential dissipation upon prolonged exposure (Figure 2B) and in dose-dependent

Figure 2. Evaluation of the impact of inhibitory compounds on *H. pylori* respiration

(A) Chemical structures of mitochondrial respiratory chain inhibitors used for further analysis.

(B) *H. pylori* P12 was incubated with the indicated compound concentrations for 3 h, and membrane potential was determined by flow cytometry after $DiOC_2(3)$ staining. The non-specific protonophore CCCP was used as a control.

(C) Strain P12 was treated for 5 min with the indicated compounds, or with DMSO as a control, and relative bacterial ATP contents were determined. The indicated data are mean values and standard deviations from five independent experiments.

(D) Oxygen consumption of strain P12 treated with the indicated inhibitor concentrations was determined as in Figure 1E. Data represent means and SEM from four independent experiments (five independent experiments for untreated).

(E) Strain P12 was grown in liquid culture and labeled overnight with 10 mM [U-$^{13}C_6$]glucose, and metabolic signatures were determined by GC-MS analysis. Key metabolites with a ^{13}C excess higher than 1% are shown as means and standard deviations of five independent experiments.

(F) Altered ^{13}C incorporation levels obtained by isotopolog profiling after treatment with respiration inhibitors for 5 min. Data represent mean values and standard deviations of changes in the respective ^{13}C excess values (percentage increase or decrease) in comparison with untreated control from at least two independent experiments. Statistics: one-way ANOVA, Bonferroni's *post hoc* test, only significant differences indicated; *$p < 0.05$; **$p < 0.01$; ***$p < 0.001$.

(G) *H. pylori* P12[TEM-1-CagA] was co-incubated for 2.5 h with AGS cells in the absence or presence of the indicated inhibitor concentrations, and CagA translocation was determined by a TEM-1-CagA translocation assay. Data are indicated in relation to untreated control, which was set to 100%, and represent mean values and standard deviations of five independent experiments.

(H) AGS[LgBiT] cells were infected with P12[HiBiT-CagA] in a real-time translocation assay setting. After 25 min (arrow), the indicated compounds were added, and measurement of CagA translocation was continued. A representative result with means and SD from two technical replicates is shown. See also Table S3.

ATP level reduction already after a short treatment (Figure 2C). Furthermore, pre-incubation of *H. pylori* with each compound inhibited oxygen consumption, similar to the myxobacterial compounds (Figure 2D).

To obtain further evidence for the involvement of *H. pylori* complex I, we employed an isotopolog profiling approach, in which bacteria were grown in the presence of [U-$^{13}C_6$]glucose to provide isotopic steady-state conditions before adding the compounds, and ^{13}C enrichment in key cytosolic metabolites was subsequently determined via gas chromatography-mass spectrometry (GC-MS). As reported previously,[30] substantial levels of ^{13}C incorporation could be detected in metabolites such as lactate, TCA cycle intermediates, amino acids, and fatty acids (Figure 2E), of which TCA cycle intermediates and derived amino acids (Asp and Glu) were specifically expected to reflect respiratory activities. When the bacteria were treated with rotenone, antimycin A, or CCCP for 5 min, ^{13}C enrichment levels indeed changed significantly for several metabolites (Figure 2F), thus providing an instantaneous imprint of changes in the core metabolism. Equivalent treatment of *H. pylori* with DFM, FPX, or FZQ resulted in altered ^{13}C enrichment profiles similar to rotenone-treated, but distinct from antimycin A- or CCCP-treated, bacteria, further supporting the notion that these inhibitors act on complex I of *H. pylori* (Figure 2F). This conclusion is corroborated by the fact that mitochondrial complex III inhibitors were active against *H. pylori* only in the micromolar range, while partly displaying weak growth inhibition against other bacteria, whereas CCCP inhibited the growth of all species tested (Table S3). Determination of CagA translocation efficiency in the presence of DFM, FPX, or FZQ confirmed that these compounds effectively interfere with type IV secretion, like the myxobacterial compounds (Figure 2G). Adding the compounds to an ongoing type IV secretion process resulted in almost immediate termination of CagA translocation (Figure 2H), indicating rapid and direct inhibition of the secretion system, rather than indirect bactericidal effects. Collectively, these results demonstrate that mitochondrial inhibitors also act as respiratory chain inhibitors in *H. pylori* and suggest that complex I inhibition leads to species specificity.

Mutations conferring decreased sensitivity against respiration inhibitors reveal NuoB and NuoD as target proteins

To select for bacterial mutants with increased compound resistance and thus to determine the target structures of the inhibitors more directly, we exposed *H. pylori* wild-type (WT) strain P12 over multiple selection rounds to sublethal compound concentrations and obtained mutant clones with decreased sensitivity against FPX (Figure 3A). Sequencing revealed a *nuoD* V133M mutation in all mutant clones and, in some cases, an additional T27A mutation in the *nuoB* gene. Both genes are part of the *nuo* operon (*nuoA* to *nuoN*), which encodes complex I in *H. pylori*.[32] Subsequently, we transformed strain P12 with genomic DNA from these variants or with PCR products spanning different regions of the *nuo* operon. Transformation with genomic DNA, or with PCR products containing the *nuoD* gene, resulted in bacteria with similarly reduced sensitivities, confirming that the resistance phenotype is transferable with the V133M^{NuoD} mutation alone. Likewise, variants with T27N^{NuoB} mutations were identified after selection of strain P12 on medium containing DFM or FZQ (Figure 3B). This mutation resulted in minimal inhibitory concentrations (MICs) of 2–4 μM for DFM and FZQ and also conferred a 4-fold higher resistance against FPX. In contrast, the V133M^{NuoD} mutation caused a 32-fold higher resistance against FPX, but did not result in decreased susceptibility against DFM or FZQ (Figure 3C), indicating two distinct inhibition characteristics. A targeted T27A^{NuoB} single mutant generally showed weaker resistance compared with the T27N^{NuoB} mutation, but a similar overall behavior. In addition, the T27N^{NuoB} mutant (and also the T27A^{NuoB}/V133M^{NuoD} double mutant) showed a slightly decreased sensitivity toward rotenone, whereas none of these mutations conferred higher resistance against the complex III inhibitor antimycin A, as expected. Growth curves revealed that all mutant strains except T27A^{NuoB} suffered from reduced fitness, and particularly the T27N^{NuoB} mutation was associated with a severe growth defect (Figure 3D). Therefore, we used only the V133M^{NuoD} mutant for oxygen consumption and isotopolog profiling experiments to show that reduced compound sensitivity was indeed due to corresponding alterations in respiratory function. Although the V133M^{NuoD} variant showed a general decrease in oxygen consumption, compared with WT, this level could not be further inhibited by FPX, whereas the WT lost its oxygen consumption ability completely in the presence of 75 nM FPX (Figure 3E). Furthermore, while incubation with FPX caused the above-mentioned reduction of ^{13}C incorporation into several respiration-related metabolites for the WT, the V133M^{NuoD} variant showed a similar profile already in the absence of inhibitors, but no additional changes upon FPX treatment (Figure 3F). Collectively, these data illustrate that reduced FPX sensitivity of the V133M^{NuoD} variant is indeed caused by the corresponding changes in complex I.

Molecular modeling of the *H. pylori* complex I quinone-binding cavity enables rational inhibitor design

The NuoB and NuoD proteins (termed Nqo6 and Nqo4, respectively, in some bacteria) form, together with NuoH (Nqo8), the quinone reaction chamber in bacterial complex I assemblies (Figure 4A). Most complex I inhibitors, although varying widely in their chemical structures, have the common ability of interfering with the entry of quinones into this chamber.[33] Alignment of *H. pylori* NuoB with other bacterial NuoB proteins, including Nqo6 from *Thermus thermophilus*, as well as with NUKM from *Yarrowia lipolytica* and mammalian NDUFS7 (PSST) proteins, showed that T27^{NuoB} is not conserved itself, but part of a conserved region in different complex I assemblies (Figure S3A), which is located near the iron-sulfur cluster N2 and directly coordinates rotenone in the ovine complex I structure.[34] The high sequence similarities between bacterial and mitochondrial NuoB (Figure S3A), NuoD (Figure S3B), and NuoH orthologs prompted us to build five homology models of the *H. pylori* NuoB/D/H interface based on bacterial or mitochondrial structures, in which the quinone-binding site is in different conformations (Figure 4B). In all models, T27^{NuoB} and V133^{NuoD} are located at the interface between both proteins and within the deep quinone-binding site close to N2 (Figure 4C). Conceivable binding modes for inhibitors are either in this first quinone-binding site or in a second quinone-binding position, in which the quinone head group is located 2.7 nm away from N2[34–37] (Figure 4C). Using molecular docking

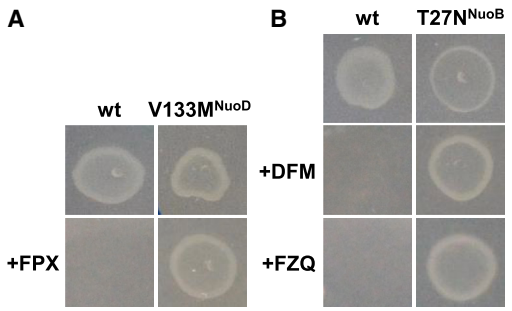

C

	DFM	FPX	FZQ	rotenone	antimycin A
wt	0.25 μM	0.3 μM	0.125 μM	4 μM	120 μM
T27N^{NuoB}	16xMIC$_{wt}$	4xMIC$_{wt}$	16xMIC$_{wt}$	2xMIC$_{wt}$	1xMIC$_{wt}$
T27A^{NuoB}	2xMIC$_{wt}$	4xMIC$_{wt}$	2xMIC$_{wt}$	1xMIC$_{wt}$	1xMIC$_{wt}$
V133M^{NuoD}	<MIC$_{wt}$	>32xMIC$_{wt}$	<MIC$_{wt}$	1xMIC$_{wt}$	1xMIC$_{wt}$
V133M^{NuoD}/ T27A^{NuoB}	<MIC$_{wt}$	>32xMIC$_{wt}$	<MIC$_{wt}$	2xMIC$_{wt}$	1xMIC$_{wt}$

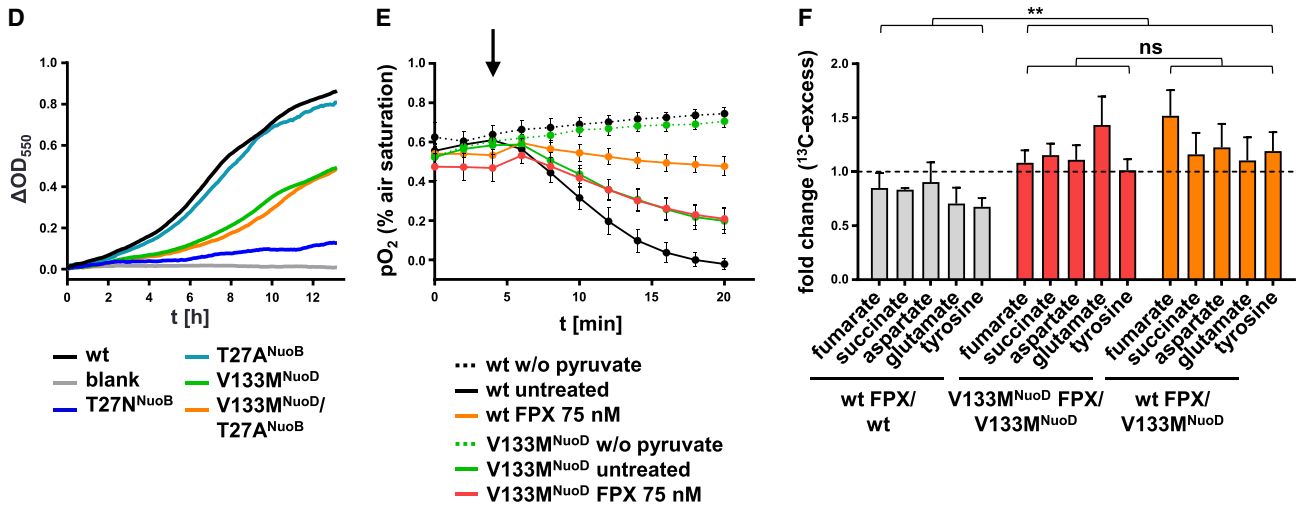

Figure 3. Target identification of respiratory inhibitors

(A) Growth of strain P12 and a V133M^{NuoD} variant on serum agar plates or plates containing 0.3 μM FPX.

(B) Growth of strain P12 and a T27N^{NuoB} variant on serum agar plates or plates containing either 0.25 μM DFM or 0.125 μM FZQ.

(C) MIC values of the indicated compounds for growth of P12 WT or the indicated mutants, obtained by spotting the strains on medium containing the respective compounds. Data were determined from three independent experiments.

(D) Growth of P12 and the indicated mutants was monitored as OD_{550}, as in Figure 1C.

(E) Oxygen consumption by strain P12, or the V133M^{NuoD} variant, was measured with or without FPX treatment, as in Figure 1E. Means and SEM from four independent experiments are shown.

(F) Strain P12 or the V133M^{NuoD} variant was treated with 50 nM FPX, or left untreated, and isotopolog profiles of key metabolites were determined as in Figure 2E. ^{13}C excess values were compared by calculating mean fold changes and SEM between FPX-treated samples and the indicated untreated controls, obtained from three independent experiments. Statistics: one-way ANOVA, Bonferroni's *post hoc* test, **p < 0.01.

algorithms, we calculated the most likely binding positions of inhibitory compounds FZQ, DFM, FPX, and piericidin A in the different homology models (Figures 4D and S4A–S4D). Comparison of piericidin A binding modes from the docking runs and from the *T. thermophilus* structure was used as a validation of the procedure (Figure S4A). We found that binding poses heavily depend on the conformation of loops within the quinone-binding cavity. For instance, docking modes of FZQ in the model based on *T. thermophilus* complex I bound to piericidin A in the main binding site (PDB: 6Q8O) showed the main cluster in the first binding site near Y85^{NuoD}, with the ligand pointing toward T27^{NuoB} (Figure 4D). In contrast, docking runs for the models based on *Y. lipolytica* complex I bound to ubiquinone-9 (PDB: 6RFR), or on murine complex I with an inhibitor in the second binding site (PDB: 7B93), showed FZQ mainly between the first and the second quinone-binding positions, pointing either toward T27^{NuoB} or into the quinone exit channel (similar to UQ-9 in the *Y. lipolytica* structure) (Figures 4D and S4B). Similar results were obtained in the docking runs for FPX and DFM (Figures S4C and S4D), except that the main cluster in the first binding site showed a close interaction of FPX with V133^{NuoD} (Figure S4C). These results are consistent with the concept that inhibitors can bind to both binding sites, albeit with different affinities.[34]

With these predictions, we decided to determine the inhibitory potential of a wider range of DFM, FPX, and FZQ compound analogs to obtain corresponding structure-activity relationship (SAR) data. Overall, we used 97 analogs in growth measurements at different concentrations and subsequently evaluated all compounds with MIC values up to 10 μM in further dilution steps to determine their IC_{50} values (Table S4 and Figure S4E). FZQ analogs showed very high potencies, with IC_{50} values in the low nanomolar or even subnanomolar range. Comparison of the compound structures indicated that the linker between the quinazoline moiety and the phenyl group, as well as the nature and

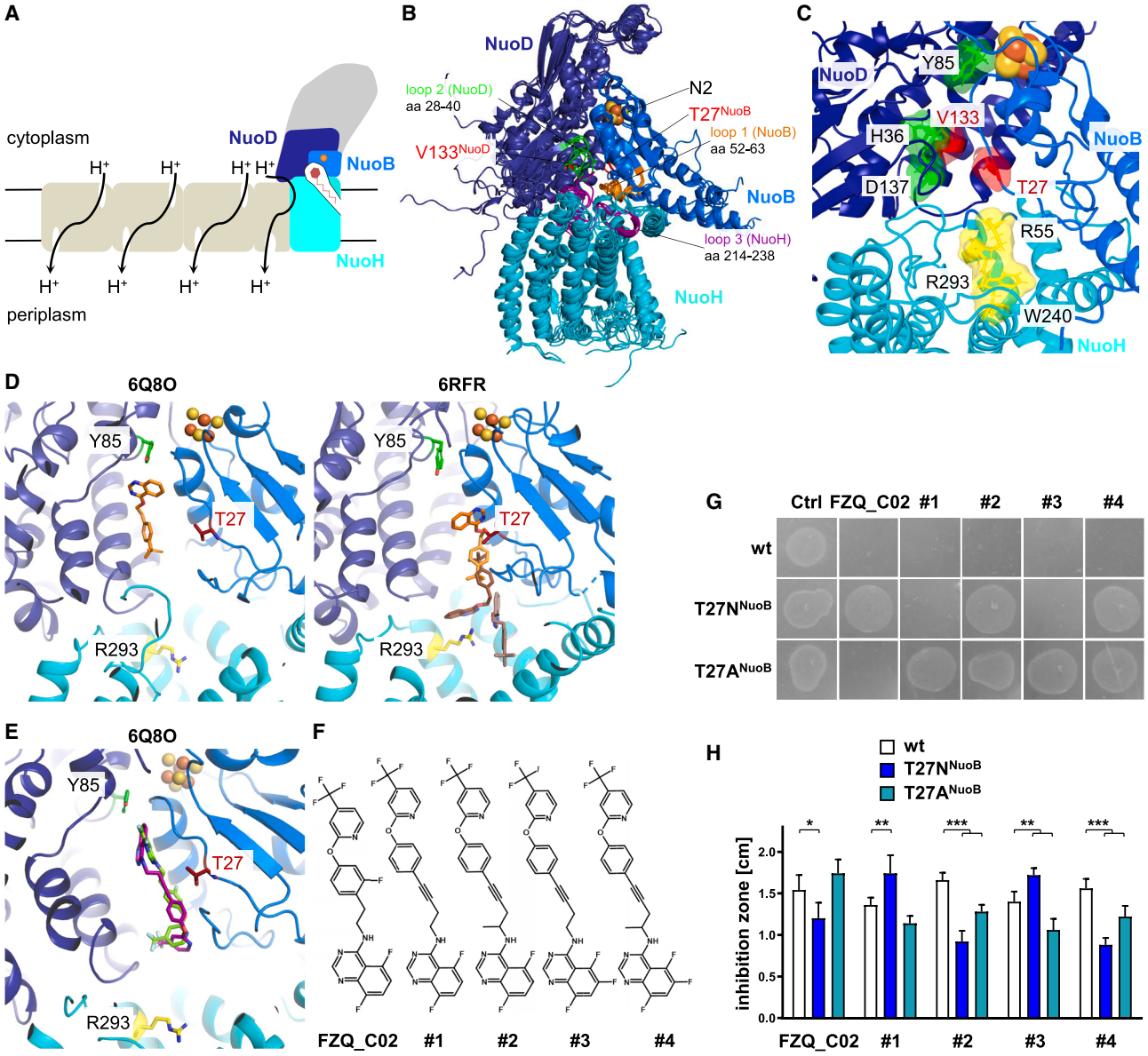

Figure 4. Molecular modeling of the *H. pylori* complex I quinone-binding site and rational design of inhibitory compounds

(A) Schematic illustration of the complex I structure. Approximate positions of NuoB, NuoD, NuoH, and the quinone-binding pocket are shown. Electrons transferred from NADH or reduced flavodoxin to iron-sulfur cluster N2 (orange dot) are used to reduce quinone within this pocket and to couple reduction with proton pumping via the integral membrane subunits.

(B) Superposition of five structural models of the *H. pylori* NuoB-NuoD-NuoH subcomplex. Three loops protruding into the quinone-binding cavity, which account for the most prominent variations between the models, and the positions of iron-sulfur cluster N2, $T27^{NuoB}$, and $V133^{NuoD}$ are indicated.

(C) Enlarged view of the quinone-binding pocket in the model based on *T. thermophilus* complex I, with $T27^{NuoB}$ and $V133^{NuoD}$ indicated as red surface and conserved residues forming the first and second quinone-binding sites indicated as green and yellow surface, respectively.

(D) Docking poses of FZQ (orange) in the homology models based on *T. thermophilus* (6Q8O) and *Y. lipolytica* (6RFR). $T27^{NuoB}$, $Y85^{NuoD}$, and $R293^{NuoH}$ are shown as red, green, and yellow stick representations, respectively.

(E) Docking poses of FZQ-C02 (green) and FZQ-C02 analog 1 (purple) in the *T. thermophilus* (6Q8O) homology model. Key residues are highlighted as in (D).

(F) Chemical structures of FZQ-C02 and of derivatives (1 to 4) containing a 3-butynylamino instead of an ethylamino linker region.

(G) Growth of strain P12, and the $T27N^{NuoB}$ and $T27A^{NuoB}$ variants, on serum agar plates containing the indicated concentrations of FZQ-C02 and its analogs 1 to 4.

(H) Sensitivity of strain P12, or $T27N^{NuoB}$/$T27A^{NuoB}$ variants, was measured as inhibition zone diameters on serum agar plates with the indicated compounds spotted on diffusion disks. Mean values and standard deviations of inhibition zone diameters from five independent experiments are indicated. Statistics: one-way ANOVA, Dunnett's *post hoc* test; *$p < 0.05$; **$p < 0.01$; ***$p < 0.001$; only significant differences are indicated. See also Figures S3 and S4 and Table S4.

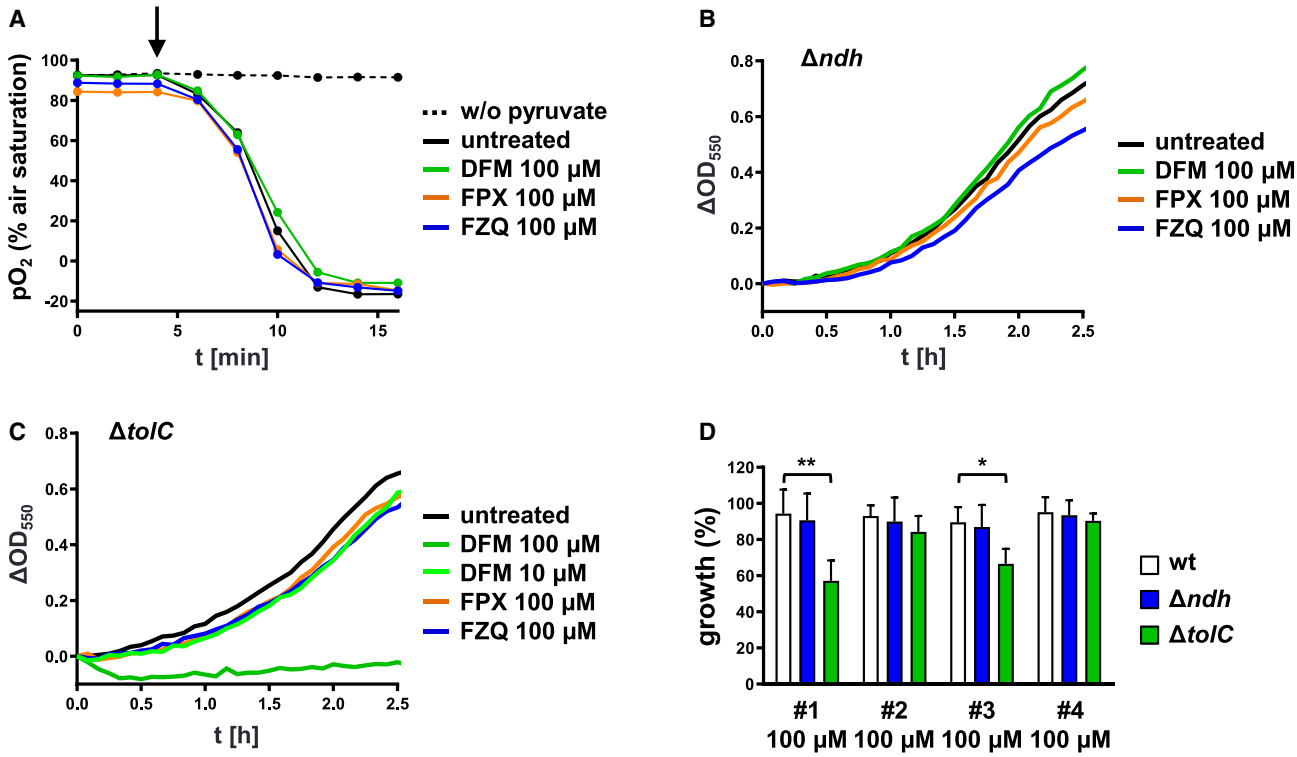

Figure 5. Examination of complex I inhibitor insensitivity in *E. coli*

(A) *E. coli* Top 10 was treated with the indicated inhibitor concentrations in OxoPlates or left untreated. Subsequently, partial oxygen pressures (pO_2) were recorded after pyruvate injection (arrow), as in Figure 1E.

(B) Growth curve of an *ndh* mutant of *E. coli* Top 10 in the presence of the indicated compounds, recorded as in Figure 1D.

(C) Growth curves of a *tolC* mutant of *E. coli* BW25113 in the presence of the indicated inhibitors, recorded as in Figure 1D.

(D) Sensitivity of *E. coli ndh* (Top 10) or *tolC* mutants (BW25113), and of their respective wild types, was measured by inhibition zone diameters in a disk diffusion assay with the indicated compounds. Data represent means and standard deviations from five independent experiments. Statistics: one-way ANOVA, Dunnett's *post hoc* test; *$p < 0.05$; **$p < 0.01$; only significant differences are indicated. See also Table S5 and Figure S5.

bulkiness of substituents on this phenyl group, is important for high inhibitory potential (Figure S4F). Compounds with the highest potency shared an ethylamino linker region, and docking runs for one such compound, FZQ-C02, indicated a positioning of the adjacent phenyl group close to $T27^{NuoB}$ (Figure 4E), which may explain the decreased sensitivity of the more voluminous variant $T27N^{NuoB}$ to this compound. To corroborate this conclusion, we selectively analyzed four further derivatives of FZQ-C02, in which the ethylamino linker between the quinazoline and the trifluoromethyl-pyridyl-oxyphenyl moieties was replaced by a butynylamino linker (Figure 4F), reasoning that an extended linker should move the phenyl group farther away from $T27^{NuoB}$, so that the corresponding molecules might fit better into the narrower quinone entry channel present in the $T27N^{NuoB}$ variant (Figure 4F). Indeed, two of these analogs (FZQ-C02#1 and FZQ-C02#3) prevented growth of the $T27N^{NuoB}$ variant in the same way as growth of the WT (Figure 4G), and showed, unlike FZQ-C02, enlarged inhibition zones for $T27N^{NuoB}$ in disk diffusion assays, thus overcoming the increased resistance of $T27N^{NuoB}$ (Figure 4H). In contrast, none of the FZQ-C02 analogs showed an activity superior to FZQ-C02 against the $T27A^{NuoB}$ variant. Strikingly, a methyl group at C-1 of the linker chain, which might increase its bulkiness (FZQ-C02#2 and FZQ-C02#4), reduced the inhibitory activity against the $T27N^{NuoB}$ and $T27A^{NuoB}$ variants. Collectively, these results strongly support the validity of our docking models and demonstrate the feasibility of structure-informed drug design to overcome potential resistance development against these inhibitors.

The extreme sensitivity of *H. pylori* toward complex I inhibitors is caused by its unique quinone-binding pocket

The observation that *H. pylori* is much more sensitive against complex I inhibitors than other bacteria led us to examine plausible reasons for the (relative) complex I inhibitor resistance in other bacteria. Facultative anaerobes, such as *E. coli*, might generally grow independent of aerobic respiration, but oxygen consumption of *E. coli* cells upon feeding with pyruvate remained unchanged in the presence of complex I inhibitors (Figure 5A). Similar to many other bacteria, *E. coli* contains a type II NADH:ubiquinone oxidoreductase (NDH-2), which transfers electrons to the respiratory chain independent of complex I and without translocating protons.[38] To examine its potential relevance, we inactivated the *ndh* gene in *E. coli* and compared the sensitivity of the resulting mutant against complex I inhibitors. However, we did not find an increased sensitivity

(Figure 5B), and thus no obvious contribution of NDH-2 to the resistance phenotype, indicating that *E. coli* complex I itself is not strongly affected by these inhibitors. However, when we used an *E. coli tolC* mutant, which is generally more sensitive to different antibiotics due to reduced efflux capabilities,[39] we found a growth defect in the presence of high DFM concentrations (Figure 5C), albeit not in the presence of FPX or FZQ. This again suggested that *E. coli* survives complex I inhibitors because of altered complex I structural details compared with *H. pylori*. Intriguingly, *E. coli* NuoB contains an asparagine residue at the position analogous to T27^{NuoB} of *H. pylori* (Figure S3A). To examine its potential relevance, we tested the sensitivity of *E. coli* WT and its *ndh* or *tolC* mutants against the FZQ-C02 butynylamino analogs shown in Figure 4F. Interestingly, analogs FZQ-C02#1 and FZQ-C02#3, but not FZQ-C02#2 and FZQ-C02#4, were able to suppress the growth of the *tolC* mutant significantly (Figure 5D), indicating that *E. coli* complex I inhibition is achievable if compounds overcoming the intrinsic N27^{NuoB} resistance reach sufficient intracellular concentrations. These results suggest that the major reason for *H. pylori* hypersusceptibility to complex I inhibitors is a combination of inefficient compound efflux and specific structural elements within the complex I quinone-binding pocket.

To identify further potential *H. pylori* variants with altered compound sensitivities due to changes in their complex I quinone-binding pocket, we searched publicly available *H. pylori* genome sequences for polymorphisms in the NuoB and NuoD proteins. Of a multitude of variants in both sequences, only a few were located within or close to the quinone-binding pocket in our models (Table S5). Based on these naturally occurring variants, and two additional NuoD variants reported recently to cause reduced sensitivity to thienopyrimidine inhibitors,[40] we generated plasmids containing the respective mutations and transformed *H. pylori* with selection on DFM, FPX, FZQ, the thienopyrimidine analog DQA5, or the synthetic aureothin derivative compound 7[41] (Table S3). In this way, we obtained a further 11 mutants (S35T^{NuoD}, S35C^{NuoD}, G37A^{NuoD}, F129L^{NuoD}, S132G^{NuoD}, D137E^{NuoD}, I397L^{NuoD}, T400I^{NuoD}, A402P^{NuoD}, F404L^{NuoD}, and a T400I^{NuoD}/A402P^{NuoD} double mutant) with increased resistance toward several compounds (Figure S5). Particularly, variants S35T^{NuoD} and G37A^{NuoD} caused a substantial resistance against DFM, FPX, and compound 7. Importantly, however, none of these mutations caused an increased resistance against FZQ. Interestingly, some of the amino acid exchanges causing reduced sensitivity of *H. pylori* (F129L^{NuoD}, T400I^{NuoD}, and F404L^{NuoD}) are already present in WT NuoD sequences of *E. coli* or *C. jejuni* (Figure S3B), indicating that the quinone-binding pocket of these bacteria may naturally be less sensitive to complex I inhibitors.

Complex I inhibitors have the potential to be developed as specific antibacterial agents (pathogen blockers) against *H. pylori*

Finally, we asked whether the high sensitivity of *H. pylori* against complex I inhibitors might be exploited to develop narrow-spectrum or species-specific antibacterials with promising characteristics. Insecticidal or acaricidal complex I inhibitors such as DFM, FPX, and FZQ were optimized to have low cytotoxicity for plant or mammalian cells, taking advantage of the generally increased sensitivity of insect mitochondria toward complex I inhibition.[42] Thus, they exhibited only moderate toxicity for L929 cells (Figure S6), and respiratory inhibition in these cells was apparent only at rather high concentrations (Figure 6A), confirming that *H. pylori* is much more sensitive to these compounds than mammalian cells.

To estimate rates of resistance development, we employed a protocol in which *H. pylori* was exposed to compound concentrations 4-fold above the respective MIC values. Under these conditions, no spontaneous mutants with resistance against FZQ were observed among pools of 10^9 bacteria, whereas mutants with resistance against FPX were obtained at a frequency of 5.5×10^{-8} (Figure 6B). In comparison, resistance against rifampicin emerged at a rate of 6.1×10^{-7} under the same conditions and resistance against the *H. pylori* eradication therapy component metronidazole at a rate of 1.2×10^{-7} (Figure 6B). Since spontaneous FZQ-resistant colonies were not obtained at 1.25 × MIC either, the emergence of a T27N^{NuoB} mutant was estimated to be very unlikely, probably due to its severe growth defect.

As a further step to assess species specificity of the complex I inhibitors, we measured their impact on the viability of typical representatives of the human intestinal microbiota. Similar to their lack of toxicity against *C. jejuni*, *E. coli*, and *S. aureus* (Table S3), DFM, FPX, and FZQ did not interfere with growth of these intestinal bacteria, even at comparably high concentrations (Figure 6C). Furthermore, we confirmed that these inhibitors were similarly active against *H. pylori* isolates that were resistant to metronidazole, tetracycline, clarithromycin, and/or amoxicillin (Figure 6D). Collectively, these observations highlight the excellent potential of complex I inhibitors to be developed as *H. pylori*-specific antibacterial agents.

DISCUSSION

The results of this study show that *H. pylori* is exceedingly sensitive to respiratory complex I inhibitors. In fact, a substantial number of small-molecule inhibitors that were obtained during a study to identify antivirulence compounds against the Cag T4SS of *H. pylori* turned out to be respiration inhibitors. This implies that the Cag type IV secretion machinery itself is highly sensitive to inhibition of the respiratory chain, which probably represents a major pathway for ATP generation and constitutes the source of the bacterial membrane potential. Administration of the identified inhibitors resulted in fast changes in profiles of ^{13}C incorporation into metabolites of the *H. pylori* central intermediary metabolism,[30] similar to those obtained with a known complex I inhibitor, suggesting that interference with complex I function leads to redirected metabolic fluxes. Furthermore, the inhibitors caused an almost immediate reduction in oxygen consumption and a rapid ATP depletion, but had a more delayed and comparatively slight impact on the membrane potential. This suggests that type IV secretion strongly depends on bacterial cell ATP levels, a conclusion that has similarly been drawn from experiments with the VirB/D4 T4SS of *Agrobacterium tumefaciens*, where ATP sensing by the cytosolic ATPases VirB11 and VirD4 was concluded to result in translocation activation.[43] Importantly, adding respiration inhibitors to an ongoing infection rapidly blocked CagA translocation, similar to high doses of the type IV secretion-disrupting agent cisplatin,[26] whereas treatment with the protein biosynthesis inhibitor erythromycin resulted in rather

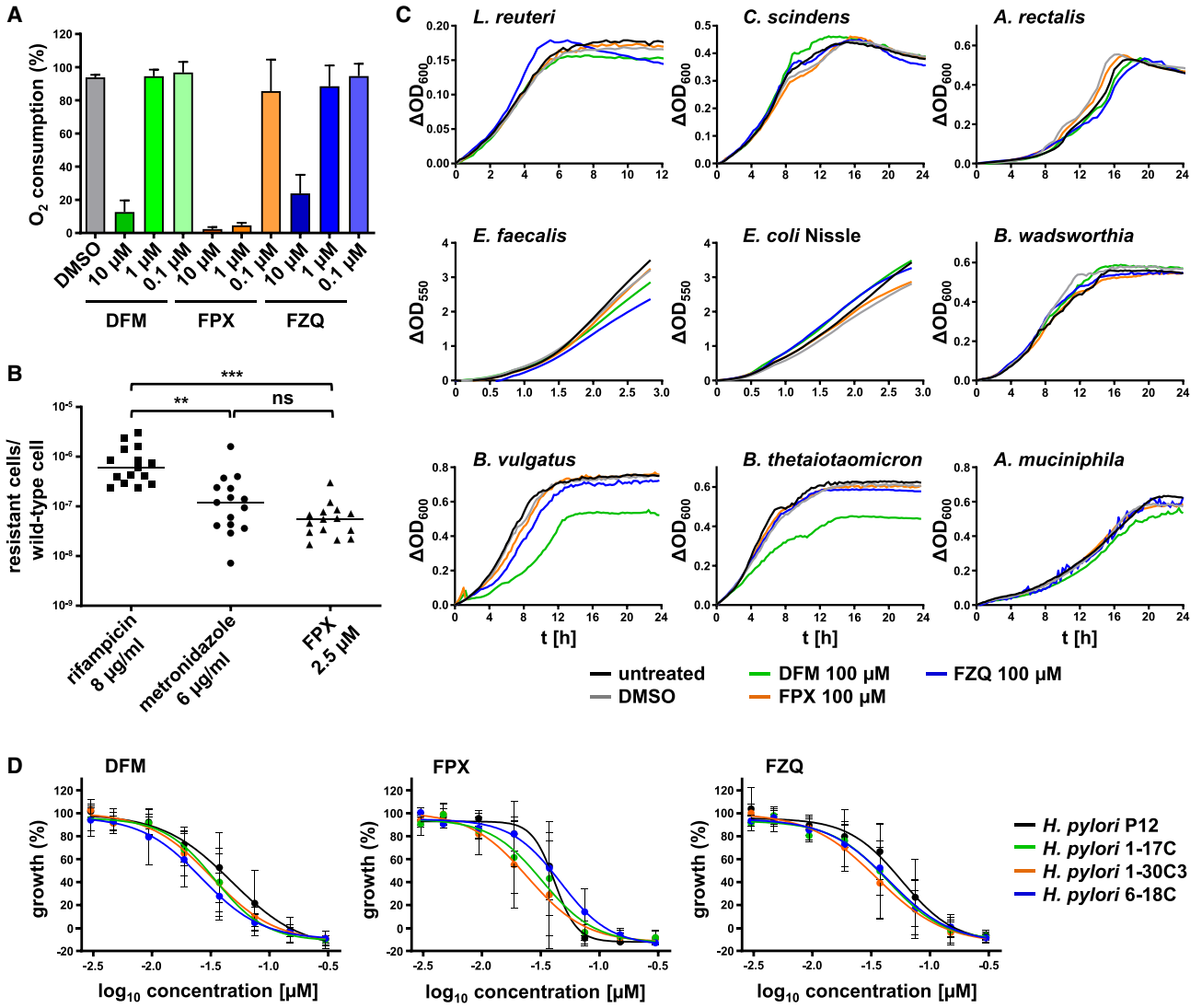

Figure 6. Activity of complex I inhibitors toward eukaryotic and prokaryotic target cells

(A) L929 cells were placed in OxoPlates and treated for 10 min with DFM, FPX, or FZQ at the indicated concentrations. Subsequently, oxygen consumption was determined. Data are indicated as percentages of untreated control and represent mean values and standard deviations of three independent experiments.

(B) *H. pylori* P12 grown for 2–3 days without selection was suspended and plated on serum agar containing the indicated compounds (equivalent to 4 × MIC for each compound). Numbers of emerging resistant colonies were divided by the respective numbers of viable bacteria grown on inhibitor-free plates. Statistics: one-way ANOVA, Bonferroni's *post hoc* test; **$p < 0.01$; ***$p < 0.001$.

(C) Growth curves of the Firmicutes species *Lactobacillus reuteri*, *Clostridium scindens*, *Agathobacter rectalis*, and *Enterococcus faecalis*; the Proteobacteria species *Escherichia coli* (Nissle) and *Bilophila wadsworthia*; the Bacteroidetes species *Bacteroides vulgatus* and *Bacteroides thetaiotaomicron*; and the Verrucomicrobia species *Akkermansia muciniphila* in the presence or absence of DFM, FPX, or FZQ (at 100 µM each).

(D) Growth inhibition diagrams of *H. pylori* P12 and multiresistant isolates 1-17C, 1-30C3, and 6-18C in the presence of DFM, FPX, or FZQ. Data represent means and standard deviations from five independent experiments. See also Figure S6.

mild short-term reduction of CagA translocation levels, while efficiently killing *H. pylori* only upon prolonged exposure. Collectively, this indicated that type IV secretion inhibition is directly associated with respiratory activity.

Although we initially identified natural complex I inhibitors as compounds affecting type IV secretion activity, one of the surprising observations of this study was that *H. pylori* is in general highly sensitive against complex I inhibitors, whereas other bacteria, including *C. jejuni*, display moderate sensitivities at most. This is not unexpected for *S. aureus*, which is known to lack a classical complex I assembly,[44] but many other bacteria, including some Firmicutes species, do contain complex I orthologs.[45] Generally, bacterial complex I assemblies comprise 14 subunits (encoded by the *nuoA* to *nuoN* genes), two of which (NuoC and NuoD) are in some cases (for instance, in *E. coli*) fused to a single protein.[45] Specific properties of *H. pylori* complex I, like in other Campylobacterota species, are a replacement of *nuoE* and *nuoF* by different genes,[45,46] which probably encode an alternative module

that accepts flavodoxin, rather than NADH, as an electron donor[47] and the exclusive utilization of menaquinone (predominantly MK-6) instead of ubiquinone as the isoprenoid quinone for respiration.[48]

Furthermore, the *H. pylori* respiratory chain is considered a simple system, with no branching of pathways[49] and comparably few metabolites used as electron donors for respiration.[29] However, complex III inhibitors were not particularly effective in *H. pylori*, and an *E. coli ndh* mutant was still resistant against complex I inhibitors, arguing against missing redundancy in the respiratory chain as a major factor for the observed hypersensitivity. Instead, the unique composition and structure of the complex I quinone-binding pocket in *H. pylori* emerge as central factors. Complex I components in *H. pylori* are generally well conserved, also in comparison with the corresponding proteins of the much larger mitochondrial complex I, which comprises the same 14 core subunits and 31 additional structural subunits.[50] Our models of the *H. pylori* complex I quinone-binding pocket, formed by NuoB, NuoD, and NuoH, show a narrow entry channel and a spacious inner cavity with a quinone reduction site close to iron-sulfur cluster N2 and a second quinone-binding site.[36,37] Quinone-analogous inhibitors such as piericidin A bind within this pocket to the first quinone-binding site.[51,52] However, the same, or other, inhibitory compounds, which may have widely different structures and little resemblance to quinone substrates,[53,54] may also bind in the second binding site or within the long entry channel.[34,52] Our modeling data indicate the potential binding of inhibitory compounds in either binding site, depending on the structure used for model building, consistent with the observation that the structure of the quinone-binding pocket changes during substrate or inhibitor occupancy.[55] For inhibitors from the FPX series, the reduced sensitivity of the $V133M^{NuoD}$ variant (and the minor influence of a $T27N^{NuoB}$ mutation) shows that inhibition is based on interactions in the first binding site. In contrast, inhibition by DFM and FZQ series compounds seems to be rather based on interactions between the first and the second quinone-binding sites. Our structure-activity relationships suggest that high inhibitory potency of compounds from the FZQ series corresponds to the presence of a chain of aromatic rings, which is in line with a recent observation that certain compounds may preferentially use aromatic residues as π-stacking partners for high-affinity binding in the second binding site.[56] However, this principle does not hold true for heterocyclic aromatic substituents in the FZQ derivatives.

Using sublethal concentrations of individual compounds, i.e., under conditions favoring the emergence of mutations in direct target genes, rather than metabolic alterations,[57] we obtained several mutants with reduced compound sensitivities. All mutations could be mapped to the complex I quinone-binding pocket, reinforcing the conclusion that its unique composition and structure lead to high sensitivity. None of the mutations described earlier to provide decreased sensitivity against benzimidazole or thienopyrimidine inhibitors[40,58] was sufficient to increase resistance against quinazoline inhibitors such as FZQ. The only mutation conferring a resistance against this compound class ($T27N^{NuoB}$) was also the one with the most severe growth defect, which is probably the reason it did not develop spontaneously under FZQ selection pressure and why it does not seem to occur naturally within the *H. pylori* population. Moreover, we demonstrate the feasibility of structure-informed drug design with FZQ modifications that overcome the resistance of this variant. Collectively, our results suggest that species specificity of the inhibitors for *H. pylori* is most likely due to its unique quinone-reaction chamber, possibly in conjunction with a weak efflux activity. An open question is why this particular composition of the complex I quinone-binding pocket, concomitant with inhibitor hypersensitivity, has evolved in *H. pylori*. Possibly, it provides an additional selective advantage for bacteria using this subgroup of complex I assemblies, which relies on a flavodoxin-oxidizing module, a NuoG protein containing an additional iron-sulfur cluster,[59] and a low-potential quinone (menaquinone MK-6). Also, the shorter quinone hexaprenyl tail, compared with the longer menaquinone or ubiquinone tails in most other bacteria,[60] might play a role. Thus, respiration might be possible at higher efficiency in the microenvironments that *H. pylori* encounters during infection or transmission, while this complex I assembly might be stable only in a protected evolutionary niche that prevents contact with microorganisms producing complex I inhibitors.

Taken together, these results show that respiratory complex I inhibitors are highly promising candidates to be developed as species-specific antibacterials against *H. pylori*. They show no cross-resistance with currently used eradication therapy drugs, are equally or even less prone to resistance development, and have a strongly reduced impact on the gastrointestinal microbiota. The extreme sensitivity of *H. pylori* to 4-aminoquinazoline compounds opens up the possibility of reaching a high therapeutic index with low mitochondrial toxicity. Other respiratory chain inhibitors used in therapeutic settings against infectious agents, such as the complex III inhibitor atovaquone[61] or the non-competitive biguanide complex I inhibitors metformin and proguanil,[62] demonstrate the principal feasibility of specifically interfering with such targets.

Limitations of the study

Antibacterial activities of the analyzed compounds are limited to single bacterial strains. Therefore, apart from potential limitations originating from *in vivo* pharmacokinetics parameters, the compounds might also act differently on a complex gastrointestinal microbiota under *in vivo* conditions.

SIGNIFICANCE

The emergence of antibiotic resistance among pathogenic bacteria highlights the importance of identifying additional drug targets. Here, we show that the Cag T4SS of *H. pylori* is highly sensitive to inhibition by natural compounds targeting mitochondrial respiration and describe a range of respiratory complex I inhibitors interfering with *H. pylori* viability at non-toxic concentrations for mammalian cells and many other bacteria. This species-specific hypersusceptibility thus emerged as a general concept with potential for the development of tailored drugs. Structure-activity relationships revealed compounds with extreme potency and distinct susceptibility profiles. Generation of bacterial mutants with decreased sensitivity and molecular modeling and docking experiments led to a detailed map of the *H. pylori* complex I quinone-binding pocket, showing that its unique molecular composition causes the extraordinary

susceptibility and makes it a promising target for development of narrow-spectrum antibiotics.

STAR★METHODS

Detailed methods are provided in the online version of this paper and include the following:

- KEY RESOURCES TABLE
- RESOURCE AVAILABILITY
  - Lead contact
  - Materials availability
  - Data and code availability
- EXPERIMENTAL MODEL AND SUBJECT DETAILS
  - Bacterial strains
  - Cell lines
- METHOD DETAILS
  - Chemicals
  - TEM-1 type IV secretion reporter assay
  - Growth curves and MIC/IC_{50} determination
  - Plasmids and transformation of *H. pylori*
  - Cross-resistance and disk diffusion assays
  - Determination of resistance development rates
  - Oxygen consumption
  - Determination of membrane potential
  - ATP content measurements
  - Isotopolog profiling
  - HiBiT-CagA translocation assay
  - Cytotoxicity
  - Molecular modeling and *in silico* docking
- QUANTIFICATION AND STATISTICAL ANALYSIS

SUPPLEMENTAL INFORMATION

Supplemental information can be found online at https://doi.org/10.1016/j.chembiol.2023.04.003.

ACKNOWLEDGMENTS

We thank Evelyn Weiss for excellent technical assistance, Jennifer Herrmann and Susanne Kirsch-Dahmen for compound library management and supply, Mark Brönstrup and Thomas Hesterkamp for support during assay development and follow-up studies, Benjamin Merget for support in model building, Wassilios Grammenos for synthesis of compound derivatives, and Barbara Schmidinger, Florenz Sasse, and Alexander Herrmann for helpful discussions. This work was supported by grants from the German Center for Infection Research (DZIF), projects 06.801, 06.810, and 06.821.

AUTHOR CONTRIBUTIONS

Conceptualization, W.F. and R.H.; validation, C.L., F.S., and A.R.M.; formal analysis, C.L., F.S., A.R.M., T.S., W.E., U.B., G.H., M.W., and W.F.; investigation, C.L., F.S., A.R.M., T.S., and D.R.; resources, R.B.-W., B.S., U.B., and M.W.; writing – original draft, W.F.; writing – review & editing, all authors; visualization, C.L. and W.F.; supervision, W.F. and R.H.

DECLARATION OF INTERESTS

R.B.-W. is co-inventor on pending European patent application EP16720354 (patent US10421749 granted).

INCLUSION AND DIVERSITY

We support inclusive, diverse, and equitable conduct of research.

Received: September 22, 2022
Revised: February 16, 2023
Accepted: April 5, 2023
Published: April 25, 2023

REFERENCES

1. Hooi, J.K.Y., Lai, W.Y., Ng, W.K., Suen, M.M.Y., Underwood, F.E., Tanyingoh, D., Malfertheiner, P., Graham, D.Y., Wong, V.W.S., Wu, J.C.Y., et al. (2017). Global prevalence of *Helicobacter pylori* infection: systematic review and meta-analysis. Gastroenterology *153*, 420–429. https://doi.org/10.1053/j.gastro.2017.04.022.
2. de Martel, C., Georges, D., Bray, F., Ferlay, J., and Clifford, G.M. (2020). Global burden of cancer attributable to infections in 2018: a worldwide incidence analysis. Lancet. Glob. Health *8*, e180–e190. https://doi.org/10.1016/S2214-109X(19)30488-7.
3. Herrero, R., Park, J.Y., and Forman, D. (2014). The fight against gastric cancer - the IARC Working Group report. Best Pract. Res. Clin. Gastroenterol. *28*, 1107–1114. https://doi.org/10.1016/j.bpg.2014.10.003.
4. Suerbaum, S., and Michetti, P. (2002). *Helicobacter pylori* infection. N. Engl. J. Med. *347*, 1175–1186. https://doi.org/10.1056/NEJMra020542.
5. Fallone, C.A., Chiba, N., van Zanten, S.V., Fischbach, L., Gisbert, J.P., Hunt, R.H., Jones, N.L., Render, C., Leontiadis, G.I., Moayyedi, P., and Marshall, J.K. (2016). The toronto consensus for the treatment of *Helicobacter pylori* infection in adults. Gastroenterology *151*, 51–69.e14. https://doi.org/10.1053/j.gastro.2016.04.006.
6. Savoldi, A., Carrara, E., Graham, D.Y., Conti, M., and Tacconelli, E. (2018). Prevalence of antibiotic resistance in *Helicobacter pylori*: a systematic review and meta-analysis in World Health Organization regions. Gastroenterology *155*, 1372–1382.e17. https://doi.org/10.1053/j.gastro.2018.07.007.
7. Fallone, C.A., Moss, S.F., and Malfertheiner, P. (2019). Reconciliation of recent *Helicobacter pylori* treatment guidelines in a time of increasing resistance to antibiotics. Gastroenterology *157*, 44–53. https://doi.org/10.1053/j.gastro.2019.04.011.
8. Tacconelli, E., Carrara, E., Savoldi, A., Harbarth, S., Mendelson, M., Monnet, D.L., Pulcini, C., Kahlmeter, G., Kluytmans, J., Carmeli, Y., et al. (2018). Discovery, research, and development of new antibiotics: the WHO priority list of antibiotic-resistant bacteria and tuberculosis. Lancet Infect. Dis. *18*, 318–327. https://doi.org/10.1016/S1473-3099(17)30753-3.
9. Ma, Z., He, S., Yuan, Y., Zhuang, Z., Liu, Y., Wang, H., Chen, J., Xu, X., Ding, C., Molodtsov, V., et al. (2022). Design, synthesis, and characterization of TNP-2198, a dual-targeted rifamycin-nitroimidazole conjugate with potent activity against microaerophilic and anaerobic bacterial pathogens. J. Med. Chem. *65*, 4481–4495. https://doi.org/10.1021/acs.jmedchem.1c02045.
10. Then, R.L., and Sahl, H.G. (2010). Anti-infective strategies of the future: is there room for species-specific antibacterial agents? Curr. Pharm. Des. *16*, 555–566. https://doi.org/10.2174/138161210790361407.
11. Debraekeleer, A., and Remaut, H. (2018). Future perspective for potential *Helicobacter pylori* eradication therapies. Future Microbiol. *13*, 671–687. https://doi.org/10.2217/fmb-2017-0115.
12. Allen, R.C., Popat, R., Diggle, S.P., and Brown, S.P. (2014). Targeting virulence: can we make evolution-proof drugs? Nat. Rev. Microbiol. *12*, 300–308. https://doi.org/10.1038/nrmicro3232.
13. Garland, M., Loscher, S., and Bogyo, M. (2017). Chemical strategies to target bacterial virulence. Chem. Rev. *117*, 4422–4461. https://doi.org/10.1021/acs.chemrev.6b00676.
14. Theuretzbacher, U., and Piddock, L.J.V. (2019). Non-traditional antibacterial therapeutic options and challenges. Cell Host Microbe *26*, 61–72. https://doi.org/10.1016/j.chom.2019.06.004.
15. Roszczenko-Jasińska, P., Wojtyś, M.I., and Jagusztyn-Krynicka, E.K. (2020). *Helicobacter pylori* treatment in the post-antibiotics era-searching

for new drug targets. Appl. Microbiol. Biotechnol. *104*, 9891–9905. https://doi.org/10.1007/s00253-020-10945-w.

16. Cover, T.L., Lacy, D.B., and Ohi, M.D. (2020). The *Helicobacter pylori* cag type IV secretion system. Trends Microbiol. *28*, 682–695. https://doi.org/10.1016/j.tim.2020.02.004.
17. Hatakeyama, M. (2014). *Helicobacter pylori* CagA and gastric cancer: a paradigm for hit-and-run carcinogenesis. Cell Host Microbe *15*, 306–316. https://doi.org/10.1016/j.chom.2014.02.008.
18. Li, Y.G., Hu, B., and Christie, P.J. (2019). Biological and structural diversity of type IV secretion systems. Microbiol. Spectr. *7*. https://doi.org/10.1128/microbiolspec.PSIB-0012-2018.
19. Boudaher, E., and Shaffer, C.L. (2019). Inhibiting bacterial secretion systems in the fight against antibiotic resistance. Medchemcomm *10*, 682–692. https://doi.org/10.1039/c9md00076c.
20. Hilleringmann, M., Pansegrau, W., Doyle, M., Kaufman, S., MacKichan, M.L., Gianfaldoni, C., Ruggiero, P., and Covacci, A. (2006). Inhibitors of *Helicobacter pylori* ATPase Cagα block CagA transport and *cag* virulence. Microbiology *152*, 2919–2930. https://doi.org/10.1099/mic.0.28984-0.
21. Sayer, J.R., Walldén, K., Pesnot, T., Campbell, F., Gane, P.J., Simone, M., Koss, H., Buelens, F., Boyle, T.P., Selwood, D.L., et al. (2014). 2- and 3-substituted imidazo[1,2-a]pyrazines as inhibitors of bacterial type IV secretion. Bioorg. Med. Chem. *22*, 6459–6470. https://doi.org/10.1016/j.bmc.2014.09.036.
22. Shaffer, C.L., Good, J.A.D., Kumar, S., Krishnan, K.S., Gaddy, J.A., Loh, J.T., Chappell, J., Almqvist, F., Cover, T.L., and Hadjifrangiskou, M. (2016). Peptidomimetic small molecules disrupt type IV secretion system activity in diverse bacterial pathogens. mBio *7*. e00221-16. https://doi.org/10.1128/mBio.00221-16.
23. Arya, T., Oudouhou, F., Casu, B., Bessette, B., Sygusch, J., and Baron, C. (2019). Fragment-based screening identifies inhibitors of ATPase activity and of hexamer formation of Cagα from the *Helicobacter pylori* type IV secretion system. Sci. Rep. *9*, 6474. https://doi.org/10.1038/s41598-019-42876-6.
24. Lettl, C., Schindele, F., Testolin, G., Bär, A., Rehm, T., Brönstrup, M., Schobert, R., Bilitewski, U., Haas, R., and Fischer, W. (2020). Inhibition of type IV secretion activity and growth of *Helicobacter pylori* by cisplatin and other platinum complexes. Front. Cell. Infect. Microbiol. *10*, 602958. https://doi.org/10.3389/fcimb.2020.602958.
25. Schindele, F., Weiss, E., Haas, R., and Fischer, W. (2016). Quantitative analysis of CagA type IV secretion by *Helicobacter pylori* reveals substrate recognition and translocation requirements. Mol. Microbiol. *100*, 188–203. https://doi.org/10.1111/mmi.13309.
26. Lettl, C., Haas, R., and Fischer, W. (2021). Kinetics of CagA type IV secretion by *Helicobacter pylori* and the requirement for substrate unfolding. Mol. Microbiol. *116*, 794–807. https://doi.org/10.1111/mmi.14772.
27. Weissman, K.J., and Müller, R. (2010). Myxobacterial secondary metabolites: bioactivities and modes-of-action. Nat. Prod. Rep. *27*, 1276–1295. https://doi.org/10.1039/c001260m.
28. Chadwick, G.L., Hemp, J., Fischer, W.W., and Orphan, V.J. (2018). Convergent evolution of unusual complex I homologs with increased proton pumping capacity: energetic and ecological implications. ISME J. *12*, 2668–2680. https://doi.org/10.1038/s41396-018-0210-1.
29. van der Stel, A.X., and Wösten, M.M.S.M. (2019). Regulation of respiratory pathways in Campylobacterota: a review. Front. Microbiol. *10*, 1719. https://doi.org/10.3389/fmicb.2019.01719.
30. Steiner, T.M., Lettl, C., Schindele, F., Goebel, W., Haas, R., Fischer, W., and Eisenreich, W. (2021). Substrate usage determines carbon flux via the citrate cycle in *Helicobacter pylori*. Mol. Microbiol. *116*, 841–860. https://doi.org/10.1111/mmi.14775.
31. Chang, H.T., Marcelli, S.W., Davison, A.A., Chalk, P.A., Poole, R.K., and Miles, R.J. (1995). Kinetics of substrate oxidation by whole cells and cell membranes of *Helicobacter pylori*. FEMS Microbiol. Lett. *129*, 33–38. https://doi.org/10.1016/0378-1097(95)00130-W.
32. Smith, M.A., Finel, M., Korolik, V., and Mendz, G.L. (2000). Characteristics of the aerobic respiratory chains of the microaerophiles *Campylobacter jejuni* and *Helicobacter pylori*. Arch. Microbiol. *174*, 1–10. https://doi.org/10.1007/s002030000174.
33. Baradaran, R., Berrisford, J.M., Minhas, G.S., and Sazanov, L.A. (2013). Crystal structure of the entire respiratory complex I. Nature *494*, 443–448. https://doi.org/10.1038/nature11871.
34. Kampjut, D., and Sazanov, L.A. (2020). The coupling mechanism of mammalian respiratory complex I. Science *370*, eabc4209. https://doi.org/10.1126/science.abc4209.
35. Friedrich, T., van Heek, P., Leif, H., Ohnishi, T., Forche, E., Kunze, B., Jansen, R., Trowitzsch-Kienast, W., Höfle, G., Reichenbach, H., et al. (1994). Two binding sites of inhibitors in NADH: ubiquinone oxidoreductase (complex I). Relationship of one site with the ubiquinone-binding site of bacterial glucose:ubiquinone oxidoreductase. Eur. J. Biochem. *219*, 691–698. https://doi.org/10.1111/j.1432-1033.1994.tb19985.x.
36. Warnau, J., Sharma, V., Gamiz-Hernandez, A.P., Di Luca, A., Haapanen, O., Vattulainen, I., Wikström, M., Hummer, G., and Kaila, V.R.I. (2018). Redox-coupled quinone dynamics in the respiratory complex I. Proc. Natl. Acad. Sci. USA *115*, E8413–E8420. https://doi.org/10.1073/pnas.1805468115.
37. Parey, K., Haapanen, O., Sharma, V., Köfeler, H., Züllig, T., Prinz, S., Siegmund, K., Wittig, I., Mills, D.J., Vonck, J., et al. (2019). High-resolution cryo-EM structures of respiratory complex I: mechanism, assembly, and disease. Sci. Adv. *5*, eaax9484. https://doi.org/10.1126/sciadv.aax9484.
38. Kaila, V.R.I., and Wikström, M. (2021). Architecture of bacterial respiratory chains. Nat. Rev. Microbiol. *19*, 319–330. https://doi.org/10.1038/s41579-020-00486-4.
39. Li, X.Z., Plésiat, P., and Nikaido, H. (2015). The challenge of efflux-mediated antibiotic resistance in Gram-negative bacteria. Clin. Microbiol. Rev. *28*, 337–418. https://doi.org/10.1128/CMR.00117-14.
40. Mugengana, A.K., Vita, N.A., Brown Gandt, A., Moran, K., Agyapong, G., Sharma, L.K., Griffith, E.C., Liu, J., Yang, L., Gavrish, E., et al. (2021). The discovery and development of thienopyrimidines as inhibitors of *Helicobacter pylori* that act through inhibition of the respiratory complex I. ACS Infect. Dis. *7*, 1044–1058. https://doi.org/10.1021/acsinfecdis.0c00300.
41. Herrmann, A., Roesner, M., Werner, T., Hauck, S.M., Koch, A., Bauer, A., Schneider, M., and Brack-Werner, R. (2020). Potent inhibition of HIV replication in primary human cells by novel synthetic polyketides inspired by Aureothin. Sci. Rep. *10*, 1326. https://doi.org/10.1038/s41598-020-57843-9.
42. Degli Esposti, M. (1998). Inhibitors of NADH-ubiquinone reductase: an overview. Biochim. Biophys. Acta *1364*, 222–235. https://doi.org/10.1016/s0005-2728(98)00029-2.
43. Cascales, E., and Christie, P.J. (2004). *Agrobacterium* VirB10, an ATP energy sensor required for type IV secretion. Proc. Natl. Acad. Sci. USA *101*, 17228–17233. https://doi.org/10.1073/pnas.0405843101.
44. Mayer, S., Steffen, W., Steuber, J., and Götz, F. (2015). The *Staphylococcus aureus* NuoL-like protein MpsA contributes to the generation of membrane potential. J. Bacteriol. *197*, 794–806. https://doi.org/10.1128/JB.02127-14.
45. Moparthi, V.K., and Hägerhäll, C. (2011). The evolution of respiratory chain complex I from a smaller last common ancestor consisting of 11 protein subunits. J. Mol. Evol. *72*, 484–497. https://doi.org/10.1007/s00239-011-9447-2.
46. Finel, M. (1998). Does NADH play a central role in energy metabolism in *Helicobacter pylori*? Trends Biochem. Sci. *23*, 412–413. https://doi.org/10.1016/s0968-0004(98)01276-6.
47. Weerakoon, D.R., and Olson, J.W. (2008). The *Campylobacter jejuni* NADH:ubiquinone oxidoreductase (complex I) utilizes flavodoxin rather than NADH. J. Bacteriol. *190*, 915–925. https://doi.org/10.1128/JB.01647-07.

48. Marcelli, S.W., Chang, H.T., Chapman, T., Chalk, P.A., Miles, R.J., and Poole, R.K. (1996). The respiratory chain of *Helicobacter pylori*: identification of cytochromes and the effects of oxygen on cytochrome and menaquinone levels. FEMS Microbiol. Lett. *138*, 59–64. https://doi.org/10.1111/j.1574-6968.1996.tb08135.x.

49. Kelly, D.J. (2001). The physiology and metabolism of *Campylobacter jejuni* and *Helicobacter pylori*. J. Appl. Microbiol. *90*, 16S–24S. https://doi.org/10.1046/j.1365-2672.2001.01350.x.

50. Vercellino, I., and Sazanov, L.A. (2022). The assembly, regulation and function of the mitochondrial respiratory chain. Nat. Rev. Mol. Cell Biol. *23*, 141–161. https://doi.org/10.1038/s41580-021-00415-0.

51. Gutiérrez-Fernández, J., Kaszuba, K., Minhas, G.S., Baradaran, R., Tambalo, M., Gallagher, D.T., and Sazanov, L.A. (2020). Key role of quinone in the mechanism of respiratory complex I. Nat. Commun. *11*, 4135. https://doi.org/10.1038/s41467-020-17957-0.

52. Bridges, H.R., Fedor, J.G., Blaza, J.N., Di Luca, A., Jussupow, A., Jarman, O.D., Wright, J.J., Agip, A.N.A., Gamiz-Hernandez, A.P., Roessler, M.M., et al. (2020). Structure of inhibitor-bound mammalian complex I. Nat. Commun. *11*, 5261. https://doi.org/10.1038/s41467-020-18950-3.

53. Degli Esposti, M. (2015). Genome analysis of structure-function relationships in respiratory complex I, an ancient bioenergetic enzyme. Genome Biol. Evol. *8*, 126–147. https://doi.org/10.1093/gbe/evv239.

54. Murai, M., and Miyoshi, H. (2016). Current topics on inhibitors of respiratory complex I. Biochim. Biophys. Acta *1857*, 884–891. https://doi.org/10.1016/j.bbabio.2015.11.009.

55. Grba, D.N., and Hirst, J. (2020). Mitochondrial complex I structure reveals ordered water molecules for catalysis and proton translocation. Nat. Struct. Mol. Biol. *27*, 892–900. https://doi.org/10.1038/s41594-020-0473-x.

56. Chung, I., Serreli, R., Cross, J.B., Di Francesco, M.E., Marszalek, J.R., and Hirst, J. (2021). Cork-in-bottle mechanism of inhibitor binding to mammalian complex I. Sci. Adv. *7*, eabg4000. https://doi.org/10.1126/sciadv.abg4000.

57. Lopatkin, A.J., Bening, S.C., Manson, A.L., Stokes, J.M., Kohanski, M.A., Badran, A.H., Earl, A.M., Cheney, N.J., Yang, J.H., and Collins, J.J. (2021). Clinically relevant mutations in core metabolic genes confer antibiotic resistance. Science *371*, eaba0862. https://doi.org/10.1126/science.aba0862.

58. Mills, S.D., Yang, W., and MacCormack, K. (2004). Molecular characterization of benzimidazole resistance in *Helicobacter pylori*. Antimicrob. Agents Chemother. *48*, 2524–2530. https://doi.org/10.1128/aac.48.7.2524-2530.2004.

59. Gnandt, E., Dörner, K., Strampraad, M.F.J., de Vries, S., and Friedrich, T. (2016). The multitude of iron-sulfur clusters in respiratory complex I. Biochim. Biophys. Acta *1857*, 1068–1072. https://doi.org/10.1016/j.bbabio.2016.02.018.

60. Collins, M.D., and Jones, D. (1981). Distribution of isoprenoid quinone structural types in bacteria and their taxonomic implication. Microbiol. Rev. *45*, 316–354. https://doi.org/10.1128/mr.45.2.316-354.1981.

61. Nixon, G.L., Moss, D.M., Shone, A.E., Lalloo, D.G., Fisher, N., O'Neill, P.M., Ward, S.A., and Biagini, G.A. (2013). Antimalarial pharmacology and therapeutics of atovaquone. J. Antimicrob. Chemother. *68*, 977–985. https://doi.org/10.1093/jac/dks504.

62. Bridges, H.R., Jones, A.J.Y., Pollak, M.N., and Hirst, J. (2014). Effects of metformin and other biguanides on oxidative phosphorylation in mitochondria. Biochem. J. *462*, 475–487. https://doi.org/10.1042/BJ20140620.

63. Fischer, W., Windhager, L., Rohrer, S., Zeiller, M., Karnholz, A., Hoffmann, R., Zimmer, R., and Haas, R. (2010). Strain-specific genes of *Helicobacter pylori*: genome evolution driven by a novel type IV secretion system and genomic island transfer. Nucleic Acids Res. *38*, 6089–6101. https://doi.org/10.1093/nar/gkq378.

64. Harrison, U., Fowora, M.A., Seriki, A.T., Loell, E., Mueller, S., Ugo-Ijeh, M., Onyekwere, C.A., Lesi, O.A., Otegbayo, J.A., Akere, A., et al. (2017). *Helicobacter pylori* strains from a Nigerian cohort show divergent antibiotic resistance rates and a uniform pathogenicity profile. PLoS One *12*, e0176454. https://doi.org/10.1371/journal.pone.0176454.

65. Baba, T., Ara, T., Hasegawa, M., Takai, Y., Okumura, Y., Baba, M., Datsenko, K.A., Tomita, M., Wanner, B.L., and Mori, H. (2006). Construction of *Escherichia coli* K-12 in-frame, single-gene knockout mutants: the Keio collection. Mol. Syst. Biol. *2*, 2006.0008. https://doi.org/10.1038/msb4100050.

66. Stecher, B., Denzler, R., Maier, L., Bernet, F., Sanders, M.J., Pickard, D.J., Barthel, M., Westendorf, A.M., Krogfelt, K.A., Walker, A.W., et al. (2012). Gut inflammation can boost horizontal gene transfer between pathogenic and commensal *Enterobacteriaceae*. Proc. Natl. Acad. Sci. USA *109*, 1269–1274. https://doi.org/10.1073/pnas.1113246109.

67. Labigne-Roussel, A., Harel, J., and Tompkins, L. (1987). Gene transfer from *Escherichia coli* to *Campylobacter* species: development of shuttle vectors for genetic analysis of *Campylobacter jejuni*. J. Bacteriol. *169*, 5320–5323. https://doi.org/10.1128/jb.169.11.5320-5323.1987.

68. Datsenko, K.A., and Wanner, B.L. (2000). One-step inactivation of chromosomal genes in *Escherichia coli* K-12 using PCR products. Proc. Natl. Acad. Sci. USA *97*, 6640–6645. https://doi.org/10.1073/pnas.120163297.

69. Abraham, M.J., Murtola, T., Schulz, R., Páll, S., Smith, J.C., Hess, B., and Lindahl, E. (2015). GROMACS: high performance molecular simulations through multi-level parallelism from laptops to supercomputers. SoftwareX *1–2*, 19–25. https://doi.org/10.1016/j.softx.2015.06.001.

70. Sali, A., and Blundell, T.L. (1993). Comparative protein modelling by satisfaction of spatial restraints. J. Mol. Biol. *234*, 779–815. https://doi.org/10.1006/jmbi.1993.1626.

71. Haas, R., Meyer, T.F., and van Putten, J.P. (1993). Aflagellated mutants of *Helicobacter pylori* generated by genetic transformation of naturally competent strains using transposon shuttle mutagenesis. Mol. Microbiol. *8*, 753–760. https://doi.org/10.1111/j.1365-2958.1993.tb01618.x.

72. Björkholm, B., Sjölund, M., Falk, P.G., Berg, O.G., Engstrand, L., and Andersson, D.I. (2001). Mutation frequency and biological cost of antibiotic resistance in *Helicobacter pylori*. Proc. Natl. Acad. Sci. USA *98*, 14607–14612. https://doi.org/10.1073/pnas.241517298.

73. Friesner, R.A., Banks, J.L., Murphy, R.B., Halgren, T.A., Klicic, J.J., Mainz, D.T., Repasky, M.P., Knoll, E.H., Shelley, M., Perry, J.K., et al. (2004). Glide: a new approach for rapid, accurate docking and scoring. 1. Method and assessment of docking accuracy. J. Med. Chem. *47*, 1739–1749. https://doi.org/10.1021/jm0306430.

STAR★METHODS

KEY RESOURCES TABLE

REAGENT or RESOURCE	SOURCE	IDENTIFIER
Bacterial and virus strains		
H. pylori P12	Fischer et al.[63]	N/A
H. pylori P12 [TEM-1-CagA]	Schindele et al.[25]	N/A
H. pylori P12 [HiBiT-CagA]	Lettl et al.[26]	N/A
H. pylori 1-17C	Harrison et al.[64]	N/A
H. pylori 1-30C3	Harrison et al.[64]	N/A
H. pylori 6-18C	Harrison et al.[64]	N/A
E. coli TOP10	Thermo Fisher	C404003
E. coli TOP10 Δ*ndh* (CLE23)	This manuscript	N/A
E. coli BW25113	Baba et al.[65]	N/A
E. coli Δ*tolC* (JW5503-1)	Baba et al.[65]	N/A
E. coli Nissle 1917 (mutaflor)	Stecher et al.[66]	N/A
Enterococcus faecalis OG1RF	ATCC	ATCC 47077
Staphylococcus aureus Rosenbach	ATCC	ATCC 29213
Campylobacter jejuni C31	Labigne-Roussel et al.[67]	N/A
Lactobacillus reuteri I49	DSM	DSM 32035
Clostridium scindens	ATCC	ATCC 35704
Agathobacter rectalis A1-86	DSM	DSM 17629
Bacteroides vulgatus NT5001	ATCC	ATCC 8482
Bacteroides thetaiotaomicron VPI 5482	ATCC	ATCC 29148
Akkermansia muciniphila YL44	DSM	DSM 26127
Bilophila wadsworthia	DSM	DSM 11045
Chemicals, peptides, and recombinant proteins		
Antimycin A	Sigma	A8674
CCCP	Sigma	C2759
CCF4-AM	Thermo Fisher	K1029
Complex I and complex III inhibitors, see Table S3	BASF SE	N/A
DFM, FPX and FZQ analogs, see Table S4	BASF SE	N/A
Metronidazole	Cayman Chemical	9002409
MXL compound library	Helmholtz Institute for Pharmaceutical Research Saarland	N/A
Rifampicin	Sigma	R3501
Rotenone	Sigma	R8875
Critical commercial assays		
OxoPlates	PreSens	OP96U
BacLight™ Bacterial Membrane Potential Kit	Thermo Fisher	B34950
ATP Bioluminescence Assay Kit CLS II	Roche	11699695001
WST-1 cell proliferation assay	Roche	05015944001
Experimental models: Cell lines		
Human: AGS cell line	ATCC	CRL-1739; RRID:CVCL_0139
Human: AGS [LgBiT] cell line	Lettl et al.[26]	N/A
Mouse: L929 cell line (NCTC clone 929)	ATCC	CCL-1; RRID:CVCL_0462
Oligonucleotides		
Primers for generating *nuo* locus products, deleting *ndh2*, or introducing *nuoB* or *nuoD* mutations, see Table S6	This manuscript	N/A

(*Continued on next page*)

Continued

REAGENT or RESOURCE	SOURCE	IDENTIFIER
Recombinant DNA		
pKD4	Datsenko and Wanner[68]	RRID:Addgene_45605
pKD46-Δndh	Datsenko and Wanner[68]	N/A
pCL32-nuoD-T400I	This manuscript	N/A
pCL33-nuoD-A402P	This manuscript	N/A
pCL34-nuoD-T400I/A402P	This manuscript	N/A
pCL43-nuoD-F129L	This manuscript	N/A
pCL44-nuoD-S132G	This manuscript	N/A
pCL45-nuoD-D137E	This manuscript	N/A
pCL46-nuoD-I397L	This manuscript	N/A
pCL47-nuoD-F404L	This manuscript	N/A
pCL49-nuoB-P25S	This manuscript	N/A
pCL50-nuoB-C32W	This manuscript	N/A
pCL51-nuoD-S35C	This manuscript	N/A
pCL52-nuoD-G37A	This manuscript	N/A
pCL60-nuoB-F54V	This manuscript	N/A
pCL61-nuoD-F144V	This manuscript	N/A
pSMART-HP2kb03_D21	Fischer et al.[63]	N/A
pSMART-HP2kb09_J02	Fischer et al.[63]	N/A
Software and algorithms		
FlowJo 10.0	Becton Dickinson	RRID:SCR_008520
Glide	Schrödinger, LLC	RRID:SCR_000187
GraphPad Prism 9	GraphPad Software Inc.	RRID:SCR_002798
GROMACS v2021.2	Abraham et al.[69]	RRID: SCR_014565
LigPrep (2020)	Schrödinger, LLC	RRID:SCR_016746
MARS Data Analysis software	BMG Labtech	RRID:SCR_021015
Modeller 10.2	Sali and Blundell[70]	RRID:SCR_008395

RESOURCE AVAILABILITY

Lead contact

Further information and requests for resources and reagents should be directed to and will be fulfilled by the lead contact, Wolfgang Fischer (fischer@mvp.lmu.de).

Materials availability

This study did not generate new unique reagents.

Data and code availability

- All data reported in this paper will be shared by the lead contact upon request.
- This paper does not report original code.
- Any additional information required to reanalyze the data reported in this paper is available from the lead contact upon request.

EXPERIMENTAL MODEL AND SUBJECT DETAILS

Bacterial strains

H. pylori strains were grown on GC agar plates (Oxoid) supplemented with vitamin mix (1%) and horse serum (8%) (serum plates), or in *Brucella* broth (BB) supplemented with 10% FCS, and cultured for 16-60 h in a microaerobic atmosphere (85% N_2, 10% CO_2, 5% O_2) at 37 °C. *S. aureus* and *E. coli* strains were grown at 37 °C on Luria-Bertani (LB) agar plates or in LB liquid medium supplemented with antibiotics, as appropriate. *C. jejuni* was grown on serum plates or in *Brucella* broth, 10% FCS at 37°C, 10% CO_2. All other bacterial species were grown in Anaerobic *Akkermansia* Medium at 37 °C, using a 7% H_2, 10% CO_2, 83% N_2 gas mixture.

Cell lines

AGS cells (human, female) were cultivated in RPMI/10% FCS at 37 °C, 5% CO_2 in 75 cm^2 tissue culture flasks (BD Falcon) and subcultivated in 6-well, 96-well (black, transparent bottom, tissue cultured treated, 4titude), or 384-well microtiter plates (black, transparent bottom, tissue culture treated, Corning Inc.), as appropriate. For cultivation of AGS [LgBiT] cells, a stably transfected derivative of AGS cells,[26] media were supplemented with 0.5 mg/ml hygromycin. L929 cells (murine, male) were cultivated in DMEM/10% FCS supplemented with 2 mM L-glutamine and 1 mM sodium pyruvate at 37 °C, 5% CO_2.

METHOD DETAILS

Chemicals

The MXL library was provided by the Helmholtz Institute for Pharmaceutical Research Saarland (Dept. Microbial Natural Products; Saarbrücken, Germany) via the Helmholtz Center for Infection Research (Braunschweig, Germany). Compounds in this library were confirmed by MS upon generation of stock solutions. Compounds described in Table S3 were either produced as described previously,[41] obtained from commercial suppliers, as indicated in the key resources table, or provided by BASF SE (Ludwigshafen, Germany). All compounds shown in Figure 4 or Table S4 have been described previously in patents WO9404527 A1, WO2010025451 A2, or US 2016/0221964 A1 mentioned below, and/or are commercially available, and were also provided by BASF SE. Compounds provided by BASF SE were re-confirmed via LC/MS analysis with correct mass and LC purity >95%. Compound FZQ_C02 has been described in patents WO9404527 A1 (Dreikorn, B.A., et al.; Pyridylethoxy-, pyridylethylamino-, and pyridylpropyl- derivatives of quinoline and quinazoline as pesticides and agrochemical fungicides) and WO2010025451 A2 (Brewster, W., et al.; Preparation of difluoro(((heteroaryloxy)phenyl)ethylamino)quinazoline derivatives for use as fungicides, insecticides, and pesticides). Compounds FZQ-C02#1 to FZQ_C02#4 have been described in patent US 2016/0221964 A1 (Grammenos, W., et al.; Preparation of pyrimidine compounds as agricultural and horticultural fungicides).

TEM-1 type IV secretion reporter assay

For screening, compound libraries were pre-pipetted into 384-well plates (low volume, sterile, Corning Inc.) such that the well content was sufficient for a 20μL test volume, and air-dried. Suspensions of bacterial cells (*H. pylori* P12 [TEM-1-CagA]) with an OD_{550} of 0.075 in Dulbecco's PBS supplemented with 10% (v/v) FCS were added to the plates (20 μl per well) and incubated for 30 min at 37 °C and 10% CO_2. Subsequently, 17 μL of the bacteria-compound mixture was gently aspirated and transferred onto AGS cells seeded in 384-well microtiter plates. Infection was performed by incubation for 2.5 h at 37 °C, 10% CO_2. For evaluation, infected cells were loaded with CCF4-AM substrate, and TEM-1 activity was determined using a Clariostar plate reader (BMG Labtech), as described previously.[25] CagA translocation was defined as the ratio of emissions (E): [$E_{460\ nm}$ (sample) - $E_{460\ nm}$ (blank)] / [$E_{530\ nm}$ (sample) - $E_{530\ nm}$ (blank)], where the blank wells contained only CCF4-AM loading solution, but no cells or bacteria. In subsequent re-screen assays, compounds were tested in a 96-well format with different incubation and washing conditions (BAC, CELL, SCREEN layouts), as indicated in Figure S1A. All other quantitative type IV secretion measurements were performed in a 96-well format, using the SCREEN layout.

Growth curves and MIC/IC_{50} determination

Bacteria grown on agar plates were diluted to an OD_{550} of 0.075 to 0.15 in the respective media and subcultured in 96-well plates (clear, flat-bottom). Plates were sealed with a gas-permeable membrane (Breathe-Easy® sealing membrane, Diversified Biotech) and incubated at 37 °C, 200 rpm in a plate reader (Clariostar, BMG Labtech). In case of *H. pylori* and *C. jejuni*, CO_2 levels were additionally adjusted to 10% using an atmospheric control unit (BMG Labtech). Anaerobic bacteria were grown at 37°C in a plate reader (Epoch 2, Agilent) positioned in an anaerobic chamber. OD_{550} was automatically measured every 5 min until the stationary phase was reached. To evaluate the antimicrobial activity of selected compounds *in vitro*, the same experimental setup was used, with the respective compounds added to the corresponding concentrations. Inhibitors were tested in serial two-fold or ten-fold dilutions. Growth curves were processed with MARS Data Analysis software 3.30 applying a curve-smoothing factor of 21. The lowest compound concentrations that showed complete growth inhibition in five independent experiments were considered as MIC values. Additionally, MICs were evaluated for growth on serum plates supplemented with the respective compounds and antibiotics. To do so, inhibitors were either added to the agar prior to solidification, or compounds were spread on the already solid agar surface. All substances were tested in two-fold dilutions. Bacteria (OD550 = 0.1, 5 μl) were spotted on the agar and grown for 2 days at 37 °C, 10% CO_2 to obtain MIC values.

Plasmids and transformation of *H. pylori*

Plasmids pCL32 to pCL61 were generated by inverse PCR with primers nuoDmut1 to nuoD-F144V (Table S6) from gene library plasmids pSMART-HP2kb03_D21 or pSMART-HP2kb09_J02 (containing strain P12 chromosomal fragments from nucleotide 1314906 to 1317526, or from 1312897 to 1314898, respectively). *H. pylori* strain P12 was transformed using linear PCR products (obtained with primers nuoAB fwd to nuoN rev, see Table S6), plasmids pCL32 to pCL61, or genomic DNA, as described previously.[71] Briefly, bacteria were suspended in BB/10% FCS at an OD_{550} of 0.2, and incubated at 37°C, 10% CO_2 under gentle agitation for 2 h. DNA was added, and suspensions were incubated for 4 h under the same conditions, and then spread on serum agar plates containing the respective antibiotics. For selection of transformants with reduced sensitivity to respiration inhibitors, transformation mixtures were spread on serum agar plates, and sterile, 6 mm diameter paper disks were placed on these plates, and soaked with 15 μl of the

respective compound diluted to the indicated concentration in BB medium. An *E. coli* TOP10 Δ*ndh* mutant was generated with a one-step PCR-based protocol[68] using primers Δndh fwd and Δndh rev (Table S6).

Cross-resistance and disk diffusion assays

To analyze resistance patterns, *H. pylori* P12 wt, *nuoB* or *nuoD* mutant strains were collected from serum plates and suspensions were adjusted to OD_{550} = 0.1. Aliquots of 5 μl bacterial suspensions were spotted on serum plates supplemented with the desired concentrations of the compounds. Growth was checked after incubation for 2-3 days, and pictures were taken using a SLR camera (Canon). To compare the sensitivities of *H. pylori* mutants to selected small molecule inhibitors quantitatively, zones of growth inhibition were determined via disk diffusion tests. To do so, bacteria were harvested, suspensions were adjusted to OD_{550} = 0.1, and 100 μl of the respective strains were plated on non-selective serum plates. Sterile paper disks (Ø 0.6 cm) were placed on the agar, and 15 μl of the compound of interest diluted to the indicated concentration in BB medium were applied. Bacteria were grown under standard conditions for 3-4 days and the zones of inhibition were measured.

Determination of resistance development rates

A protocol adapted from[72] was used to determine the spontaneous emergence of resistance. Briefly, *H. pylori* liquid cultures were started with low amounts of bacteria (6 x 10^5 cfu) in a small volume of BB/FCS (50 μl) and grown in 96-well plates for 12 h at 37 °C, 10% CO_2 under gentle agitation. The culture volume was subsequently increased to 500 μl and finally to 10 ml in a cell culture flask (T25). After 2-3 days, bacteria in the stationary growth phase were harvested (4000 rpm, 20 min) and resuspended in 1 ml BB/FCS. Next, 100 μl were spread on serum plates supplemented with the indicated concentration of the compound of interest (this corresponds to 1 ml of the original culture). In parallel, the total number of cfu/ml was determined. Plates were incubated for 5-6 days at 37 °C, 10% CO_2, and colonies were counted. Resistance rates were computed by dividing the number of resistant colonies by the count of viable cells. The median was calculated from at least five independent experiments with three independent cultures each, so that occasional "jackpot cultures" have no influence on the statistics. Due to the minimal amount of bacteria used to inoculate the liquid cultures, the presence of resistant mutants in the initial samples was considered rather unlikely. To further prove this assumption, 6 x 10^6 cfu (i.e., ten times the inoculum), were plated on selective plates without prior liquid cultures. In five independent experiments, <10 (rifampicin), or <3 (all other compounds), colonies per plate were observed.

Oxygen consumption

OxoPlates (OP96U, PreSens) were used to monitor oxygen consumption rates. Every batch of OxoPlates was calibrated according to the manufacturer's instructions. To measure oxygen consumption of bacteria treated with small molecule inhibitors, *H. pylori* or *E. coli* were diluted to an OD_{550} of 1 in nutrient-free buffer (D-PBS), OxoPlates were filled with 140 μl bacterial suspension per well and incubated for 10 min at 37 °C in a 10 % CO_2 incubator. Subsequently, compounds were added at the desired concentrations, and incubation was continued for further 10 min. Oxygen consumption was monitored in a prewarmed plate reader (Fluostar, BMG Labtech) at 37 °C for 20-30 min using the time-resolved mode (integration start: 0 μs, integration time: 500 μs). Indicator (I_{650}) and reference (I_{590}) fluorescence values were recorded every 2 min, and partial oxygen pressures (pO_2) were calculated as percentages of values in air-saturated water. During the third cycle (i.e. after 4 min), 4 μl of a 250 mM pyruvate stock solution in D-PBS was injected. To monitor oxygen consumption of eukaryotic cells, L929 cells were harvested using trypsin-EDTA and washed twice with D-PBS. In the meantime, OxoPlates were preincubated with 70 μl D-PBS at 37 °C to allow equilibration of the optical sensor. Next, 1 x 10^6 cells/70 μl, and corresponding compound solutions were added to each well and incubated for 10 min at 37 °C. Oxygen consumption was monitored for up to 1 h, as described for bacterial samples.

Determination of membrane potential

The bacterial membrane potential was measured via flow cytometry using the BacLight™ Bacterial Membrane Potential Kit (Thermo Fisher). Briefly, *H. pylori* were diluted to a final OD_{550} of 0.075 in PBS/FCS and incubated for the indicated time with the respective compounds at 37 °C, 10% CO_2. The ionophore CCCP (Sigma) was used as a control for disruption of the membrane potential. Subsequently, 12.5 μl of the bacterial suspension were transferred to 200 μl D-PBS supplemented with 1 mM EDTA and 15 μM $DiOC_2(3)$ and stained for 30 min at 37 °C, 10% CO_2. Red and green fluorescence was measured by flow cytometry using PE and FITC settings (BD FACSCantoTM II, BD). Results were evaluated using FlowJo 10.0.

ATP content measurements

Relative cellular ATP contents were measured using the ATP Bioluminescence Assay Kit CLS II (Sigma). Briefly, 450 μl *H. pylori* suspension (OD_{550} = 0.15 in BB/FCS) was incubated with the respective compounds for 5 min at 37 °C, 10% CO_2 and subsequently harvested by centrifugation (8000 x g, 5 min). The supernatant was discarded, and the cell pellet was resuspended in 75 μl cold 100 mM Tris/HCl, 4 mM EDTA (pH 7.6). The samples were boiled for 2 min and centrifuged for 1 min at 10000 x g, 4 °C to remove cell debris. 50 μl of the ATP-containing supernatant were transferred to a 96-well plate (black, clear flat bottom, Corning) and measurement was immediately started in a plate reader (Clariostar, BMG Labtech). Bioluminescence was recorded with 1 s delay after automatic injection of 50 μl luciferase reagent per well using a signal integration time of 10 s. ATP contents were calculated as percentage of the untreated control after subtracting the blank value (100 mM Tris/HCl, 4 mM EDTA).

Isotopolog profiling

All ^{13}C labeling and isotopolog profiling experiments were essentially performed as described previously.[30] Briefly, *H. pylori* cultures were grown in the presence of 10 mM [U-$^{13}C_6$]*D*-glucose for 16 h, and then equilibrated to 10% CO_2 for 2 h. To determine the impact of small-molecule inhibitors and reference compounds on the central metabolism, bacteria were subsequently treated for 5 min with the respective compounds at the indicated concentrations, or left untreated, and harvested by centrifugation. Pellets were inactivated by freezing on dry ice and subsequent boiling, freeze-dried, and further processed and analyzed by GC/MS, as described.[30] To compensate for a growth defect of the V133M^{NuoD} variant, precultures were inoculated with an OD_{550} of 0.2 and main cultures with an OD_{550} of 0.1, respectively. Experiments were evaluated using absolute ^{13}C excess values of the respective metabolites, or by calculating the percental ^{13}C surplus values with respect to the untreated control using the equation: $\Delta^{13}C$ surplus = [(^{13}C $excess_{sample}$ - ^{13}C $excess_{control}$)/ ^{13}C $excess_{control}$] x 100.

HiBiT-CagA translocation assay

Time dependent effects of selected compounds on CagA translocation were analyzed using the split luciferase-based HiBiT-CagA translocation assay, as described recently.[26] Briefly, P12[HiBiT-CagA] cells were diluted to a final OD_{550} of 0.1 in PBS/FCS and incubated for 2 h at 10% CO_2, 37 °C. Next, AGS[LgBiT] cells seeded in 96-well plates (black, clear-flat bottom, Greiner/4titude) were infected with 40 µl bacterial culture (MOI 25) and simultaneously supplied with 10 µl furimazine substrate mixture (Promega). Luminescence values at 470 nm were recorded in a prewarmed Clariostar plate reader, with CO_2 levels adjusted to 5%, using an atmospheric control unit (BMG Labtech). After 20-25 min, measurements were shortly paused to add the respective compounds or solvents to the appropriate concentrations.

Cytotoxicity

Proliferation and viability of eukaryotic cells treated with small molecule inhibitors was assessed using the WST-1 cell proliferation assay (Roche/Sigma-Aldrich). Briefly, murine L929 fibroblasts seeded into 96-well plates (3.0 x 10^5 cells/well, black, clear flat bottom, 4titude) were cultured in Phenol red-free medium for 24 h at 37 °C, 5% CO_2. Next, test compounds or DMSO were added to the respective concentrations and incubation was continued for 3 days. WST-1 reagent was added according to the manufacturer's protocol and plates were kept at 37 °C, 5% CO_2 for 1 h. The absorbance at 450 nm and 690 nm (reference wavelength) was recorded in a plate reader (Clariostar, BMG Labtech). For evaluation, the difference of A_{450nm} and A_{690nm} was calculated, and the blank control (medium and WST-1 only) was subtracted. Percental viability was normalized to the untreated control.

Molecular modeling and *in silico* docking

We performed molecular docking to characterize the possible binding modes of the ligands in *H. pylori* complex I. As the structure *H. pylori* complex I was not available, we built 5 different models of the structure, using 5 different templates, including mouse mitochondrial complex I in the active state (PDB: 6G2J), *Y. lipolytica* complex I bound to ubiquinone-9 (UQ-9) in the second binding site (PDB: 6RFR), mouse mitochondrial complex I bound to inhibitor in the second binding site (PDB: 7B93), *T. thermophilus* complex I bound to piericidin A in the first binding site (PDB: 6Q8O), and ovine complex I in the deactivated open state (PDB: 6ZKI). The homology models were built for subunits NuoB, NuoD, and NuoH using Modeller 10.2.[70] In order to investigate the respective binding modes, compounds DFM, FPX, FZQ, piericidin A, FZQ-C02, and FZQ-C02_#1 were docked into all 5 generated *H. pylori* complex I models using Glide.[73] The initial coordinates of all ligands were generated from 2D geometry in LigPrep (Schrödinger, LLC, New York, 2020). The stereochemistry was corrected. Docking was performed over three search spaces of 35 x 35 x 35 $Å^3$ for the inner box and 45 × 45 × 45 $Å^3$ for the outer box next to each other in the Z direction to cover the whole quinone-binding cavity. The binding poses obtained from three docking runs were pooled together for each compound and then clustered using the cluster module of the Gromacs program (v2021.2) with the Jarvis-Patrick method, and a cut-off of 4 Å.[69] As a validation, we compared the binding modes of piericidin A from the docking runs and from the *T. thermophilus* complex I structure. The most populated cluster of the piericidin A binding modeled into the model built based on 6Q8O was indeed very similar to the piericidin A binding mode from the experimental structure (Figure S4A). However, the main cluster for the model built based on 6RFR (UQ-9 bound in the second binding site) shows the headgroup of piericidin A near the headgroup of UQ-9 in the original structure (data not shown).

QUANTIFICATION AND STATISTICAL ANALYSIS

Statistical analysis was performed using the GraphPad Prism 9 software. Quantitative data sets are generally shown as average values resulting from at least three independent experiments, with standard deviations, or standard errors of the mean (SEM), as indicated in the figure legends. The significance of differences was determined using One-way ANOVA, with post-hoc tests as indicated. IC_{50} values were calculated from five independent experiments using non-linear fit in Graph Pad Prism 9.